Marine Structures 108 (2026) 104011

Contents lists available at ScienceDirect

Marine Structures

journal homepage: www.elsevier.com/locate/marstruc

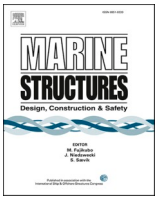

Accelerated fully coupled hydro-elastic analysis of ships using a combined full and modal-reduced FEM approach

Julio García-Espinosa [a], Antonio José Lorente-López [b,*], Borja Serván-Camas [c], José Enrique Gutierrez-Romero [b]

[a] Escuela Técnica Superior de Ingenieros Navales (ETSIN), Technical University of Madrid (UPM), Av. de la Memoria, 28040 Madrid, Spain
[b] Escuela Técnica Superior de Ingenieros Navales y Oceánicos (ETSINO), Technical University of Cartagena (UPCT), Cartagena, Spain
[c] Centre Internacional de Mètodes Numèrics en Enginyeria (CIMNE), Gran Capitan s/n, 08034 Barcelona, Spain

ARTICLE INFO

Keywords:
Modal matrix reduction
MMR
Hydroelasticity
Reduce order models

ABSTRACT

The numerical simulation of a ship's hydroelastic structural response is typically carried out using simplified modelling approaches. The main reason can be found in the computational cost of the structural solver when solving the fully coupled hydro-elastic problems. In this work, a two-way coupled fluid-structure interaction model capable of efficiently and accurately computing the hydro-elastic response of a ship using a detailed full-length structural representation is proposed. To reduce the computational cost of the structural solver, a reduced-order method based on modal matrix reduction is applied. The main idea is to largely reduce the number of degrees of freedom of the structural system by retaining only those modes with significant energy. Furthermore, to improve the accuracy of the model, this work proposes a combined methodology in which a residual finite element (FE) solution is computed alongside the reduced model, while still achieving a reduction in the overall computational effort.

The seakeeping hydrodynamics is solved using the computational framework SeaFEM. And the structural particulars are introduced into this framework to fully integrate the fluid-structure interaction.

An application case of the proposed model strategy is presented for a detailed structural design of a ship. The consistency of the modal approximation and methodology is verified against the full FE structural solution. It shows the capabilities of the proposed framework to perform a fully coupled and detailed structural analysis, instead of at component level, with a significant reduction in computational time.

1. Introduction

The first reference to hydroelasticity in ships is generally attributed to the work of Inglis in 1929 [1], who first presented the concept that ships are flexible structures that can be modelled as elastic beams. However, the foundations for computational hydro-elasticity of ships were laid by Bishop et al. in their seminal works [2,3]. Despite the significant advancements in numerical methods over recent decades, the framework established in those works remains highly relevant and can still be considered the foundation of current computational and experimental methodologies for hydro-elastic analysis of ships and offshore platforms.

* Corresponding author.
E-mail address: antonioj.lorente@upct.es (A.J. Lorente-López).

https://doi.org/10.1016/j.marstruc.2026.104011
Received 17 July 2025; Received in revised form 11 December 2025; Accepted 8 January 2026
Available online 4 February 2026

Nomenclature

Notation

α	scalar notation
$\boldsymbol{\sigma}$	vector or tensor notation
$\boldsymbol{P}$	vector notation
$\overline{\overline{\boldsymbol{M}}}$	matrix notation

General

$\nabla\cdot$	divergence operator
∇_h	gradient operator in the horizontal directions
Γ_B	wetted surface of the body (fluid-structure interface)

Hydro-elasticity

$\boldsymbol{\sigma}$	stress tensor
$\boldsymbol{b}$	mass force vector
$\boldsymbol{u}$	structural displacement vector field
$\overline{\boldsymbol{u}}$	prescribed structural displacements
$\overline{\boldsymbol{t}}$	prescribed tractions
$\overline{\overline{\boldsymbol{M}}}$	mass matrix of the FEM hydro-elasticity problem
$\overline{\overline{\boldsymbol{B}}}$	damping matrix of the FEM hydro-elasticity problem
$\overline{\overline{\boldsymbol{K}}}$	stiffness matrix of the FEM hydro-elasticity problem
$\boldsymbol{P}$	generalized fluid force vector
$\boldsymbol{F}$	generalized force vector corresponding to concentrated loads
$\boldsymbol{G}$	generalized gravitational force vector
$\boldsymbol{U}$	vector of nodal displacements and rotations of the hydro-elasticity problem
$\boldsymbol{P_S}$	vector of loads due to the hydrostatic pressure at equilibrium position
$\boldsymbol{F_S}$	vector of static concentrated loads
$\boldsymbol{P_D}$	vector of hydrodynamic loads
$\overline{\overline{\boldsymbol{D}}} = \{\boldsymbol{D}_i\}$	matrix of characteristic eigenvectors or modes of the structure
Ω_i	natural frequency of the i th mode of the structure
$\boldsymbol{Q} = \{q_i\}$	modal generalized coordinates
$\overline{\overline{\boldsymbol{A}}}$	diagonal generalized mass matrix
$\overline{\overline{\boldsymbol{Z}}}$	diagonal generalized stiffness matrix
$\overline{\overline{\boldsymbol{C}}}$	(diagonal) generalized damping matrix
$\boldsymbol{Q_R}$	modal generalized coordinates of the rigid body modes
$\boldsymbol{Q_D}$	modal generalized coordinates of the rest of modes (excluding rigid body modes)
$\boldsymbol{H_R}$	vector of generalized modal forces of the rigid body modes
$\boldsymbol{H_D}$	vector of generalized modal forces of the rest of modes
$\boldsymbol{E}^D_{MMR}$	elastic energy

Rigid-body dynamics

$\overline{\overline{\boldsymbol{M}}}_{RD}$	mass matrix associated with the rigid body degrees of freedom (DOFs)
$\overline{\overline{\boldsymbol{B}}}_{RB}$	damping matrix associated with the rigid body DOFs
$\overline{\overline{\boldsymbol{K}}}_{RB}$	hydrostatic restoring matrix associated with the rigid body DOFs
$\boldsymbol{U}_{RB}$	vector containing the components of the rigid body motion
$\boldsymbol{P}_{RB}$	vectors of integrated hydrodynamic forces and moments acting on the body
$\boldsymbol{F}_{RB}$	vectors of integrated concentrated forces and moments acting on the body
$\boldsymbol{G}_{RB}$	vectors of integrated self-weight forces and moments acting on the body

Seakeeping solver

φ	velocity potential
ξ	free surface elevation
ϕ	velocity potential of the diffracted-radiated waves
ψ	velocity potential of the incident waves
ζ	free surface elevation of the diffracted-radiated waves
η	free surface elevation of the incident waves

$\boldsymbol{U}$	velocity vector of the body
$\overline{\overline{\boldsymbol{L}}}$	Laplacian Matrix
$\boldsymbol{\Theta}_B$	vector resulting of integrating the body boundary condition
$\boldsymbol{\Theta}_{TS}$	vector resulting of integrating the transom stern boundary condition
$\boldsymbol{\Theta}_R$	vector resulting of integrating the radiation boundary condition
$\boldsymbol{\Theta}_{Z_0}$	vector resulting of integrating the free surface boundary condition

Fluid-structure interaction

$\overline{\overline{\boldsymbol{I}}}^{F\to S}$	interpolation matrix mapping fluid data onto the structure boundary
$\overline{\overline{\boldsymbol{I}}}^{S\to F}$	interpolation matrix mapping displacements onto the fluid boundary
$\boldsymbol{\Gamma}$	operator for evaluating fluid pressure
$\mathscr{E}_\Gamma$	extension operator from the rigid body solution to the boundary Γ
$\mathscr{E}_\mathscr{S}$	extension operator from the boundary Γ to the full structure
N_Γ	FEM integral operation on boundary Γ

While current rules and regulations adequately cover most aspects relevant to structural ship design, several essential issues are only vaguely addressed or rely on case-by-case approval by the authorities. Among these aspects we can highlight different phenomena involving the hydro-elastic response, such as springing, whipping and racking, resulting in dynamically induced hull stresses. In this work, modal RAOs are computed to show the importance of a fully-coupled strategy to properly capture resonance effects of the lower modes, which are responsible for springing. It is shown than these effects are noticeable in wave encountering frequencies up to three times smaller than the modal frequencies.

The abovementioned dynamic phenomena can increase significantly the hull stresses. Therefore, in certain critical cases, the quasi-static approach to hydro-elasticity employed by the current rules and design guidelines can largely underestimate the actual design loads. Hence, in some cases, it is required to study the coupled hydro-elastic response of the structure [4] by carrying out experimental tests at model scale and/or running computer analysis. There are two different methods for hydro-elastic model testing. The first one and least popular, due to its complexity and cost [5], is to build a model using some elastic material trying to scale down the elastic behaviour of the ship [6,7]. In this method, the evaluation of the vibration modes cannot be estimated properly in fully elastic models due to larger internal damping [8]. The second one (and the most popular) is to build a segmented model connected by a flexible beam with similar global elastic properties [5,9–14]. The number of segments depend on the number of displacement modes to model. The pros and cons of both methodologies were analysed and compared in [8], where the advantages of the second option are highlighted.

Anyhow, a major drawback of both testing techniques is than only global hydro-elastic effects can be modelled and measured. The only alternative to analyse more local effects is the use of numerical simulations. The numerical simulation of hydroelasticity involve the coupling between the hydrodynamics and the structural dynamics. A recent study [15] highlights the growing importance of two-way coupling methods, which account for over 75 % of the research studies. The most common simulation approach combines potential flow theory for hydrodynamics and the finite element method (FEM) for structural analysis, both using 3D elements.

The approach is to solve the hydrodynamics with 3D potential flow based on the boundary element method (BEM), and the structural dynamics with the 1D beam and 3D (solid/shell) elements models using the finite element method (FEM) [13–19]. Several works have extended the fluid dynamics model, by solving the Navier Stokes equations instead of the potential flow equations [20–22]. A recent work [18] solved the global hydro-elastic response of a S175 ship using a coupled BEM–FEM approach and compared the results against the equivalent rigid body problem. From the structural point of view, just a few authors have used more sophisticated approaches such as the 1D-3D FEM hybrid method [16,19] or directly coupling a fully 3D FEM [23]. Most of the works only consider the linear response, while the most common approach for modelling the structure is based on the superposition of modes [4,12,21,23,24], regardless the dimension of the model (1D beam or 3D). In order to be able to simulate transient or non-linear responses, it is necessary to work in the time-domain [4].

In the context of potential-flow solvers, several recent works in the field of floating wind propose a time-domain response-reconstruction approach, in which the solution is rebuilt from a series of unit load patterns [25–27]. This approximation significantly reduces the computational effort required for the structural assessment of a platform. However, its restriction to quasi-static analyses and the necessary introduction of spurious boundary conditions are major drawbacks. As an alternative, other authors have followed a different approach that requires performing the structural modal analysis and solving the wave-radiation problem for the corresponding displacement modes. The impulse response function proposed by Cummins [28] is used to transfer the results from the frequency domain to the time domain [12–14,19]. In some cases, only the rigid-body modes are considered in the wave-radiation problem [29,30]. A key limitation of these approximations is their inability to accurately capture local stresses -essential for predicting failure- which primarily depend on local strains [31]. In order to overcome this drawback, it is necessary to solve in the time-domain the full 3D coupled hydro-elastic problem. Solving the full hydroelasticity problem in the time-domain is much less

common in the literature due to its complexity and computational cost. In [32] a partitioned strategy was implemented to analyse the interaction between the free surface and the seals of a surface effect ship. The hydrodynamic model was based on potential flow with forward speed, and the results were compared with experimental tests. Subsequently, in [33], a study of the same case was presented using a RANS model to solve the fluid dynamics. However, due to its high computational cost, the analysis was limited to the symmetric dynamic response. The substantial cost associated with RANS-based solvers generally restricts their application to simple geometrical models or to configurations with significant simplifications. A comprehensive review of the state of the art on flexible fluid–structure interactions in marine applications can be found in [34].

Should a floating structure require a structural analysis, this is usually performed by introducing the precomputed external loads into a detailed FEM structural model based on the finite element method. This partitioned strategy implies solving the hydro-elastic problem in several stages and transforming the frequency-domain hydrodynamic loads into time-domain. This approach only enables for one-way (weak) coupling, which may be acceptable for very stiff structures but can lead to significant errors in many other practical cases [33]. When simulating flexible structures, the two-ways (strong) coupling should be considered to account for the added mass and damping induced by the water on the structure. However, it is the most common way to carry out hydro-elastic analysis, due to the complexity and computational cost of solving the full three-dimensional problem in the time-domain, mostly taken by the structural solver [35]. In this regard, two-way coupling algorithms are typically restricted to simple geometries, as in [36].

One of the most recent works (published by the authors) [35] proposed a full time-domain hydro-elastic model using FEM-FEM coupled approach. On the one hand, the hydrodynamics model is based on a first-order linear potential flow considering the forward speed using the double body linearization. The velocity potential is solved using FEM. On the other hand, the structural dynamics is solved using a co-rotational shell FEM model which takes into account the geometric nonlinearity due to the change of the normal direction of the elements caused by the rigid-body displacements. Although that work shows that a monolithic approach can be more computationally efficient than a partitioned one, the reported CPU times for all cases show that these full FEM-based models remain prohibitive for integration into a design cycle.

One way to reduce the cost of these models is the application of model-order reduction techniques. A very recent work [37] presents an application for structural response evaluation using a Reduced-Order Model (ROM) generated from a Krylov subspace. Although it employs a very coarse structural definition and is restricted to one-way coupling, the study shows how these techniques can deliver high accuracy while drastically reducing computational times.

In the present work, on the other hand, the rigid body displacements are solved separately from the elastic displacements, and the latter are solved in a frame of reference fix to the structural system, making the geometrical linearity valid due to the consideration of the linear elastic response.

Also in this work, we aim to go further by developing a two-way coupled fluid-structure interaction model that can efficiently and accurately compute the hydro-elastic response of a ship using a detailed full-length structural representation. For this purpose, a single FEM-based computational framework is employed, in which the structural model is strongly coupled with the time-domain seakeeping solver SeaFEM [39–44]. To reduce the computational cost of coupled problem, a ROM based on the modal matrix reduction (MMR) technique [45] is developed for the structural solver. By retaining only those eigenmodes preserving most of the structural elastic energy, the number of structural Degrees of Freedom (DOFs) is greatly reduced, which also results in a significant decrease in the computational cost of the structural solver. However, the direct application of MMR can lead to a noticeable loss of accuracy, especially in the calculation of structural details. To overcome this drawback, this work proposes a hybrid methodology in which a residual FEM solution is computed to improve the reduced model solution.

This work finally presents a case study of a ship, analyzing different conditions to evaluate its dynamic response and demonstrate the capabilities of the developed computational framework. The case study shows how the hybrid Reduced Order Model - Full Order Model (ROM - FOM) approach enables a two-orders-of-magnitude speed-up without a noticeable loss of accuracy.

2. Computational framework

As previously noted, the conventional hydro-elastic analysis approach - involving a full FEM model of the structure - remains based on the weak one-way methodology described in current rules and design guidelines, as depicted in Fig. 1. The main steps are summarized as follows:

1. In the first stage, the frequency-domain seakeeping solver solves the wave diffraction-radiation problem, from where the added mass, damping, Froude-Krylov and diffraction-radiation pressure distributions and loads are obtained.
2. In order to obtain the time dependent hydrodynamic loads, those outputs need to be transformed to the time-domain for each rigid-body dynamics realization representing a load-case.
3. Later, all external loads and the hydrodynamic pressure must be introduced into a structural solver to obtain the structural response.
4. Finally, the structural solver computes the displacements and stresses.

Several drawbacks are drawn from this methodology:

- A number of independent computational tools must be used in serial execution.
- A large number of files and data are generated. These must be stored, written and accessed by the different tools.

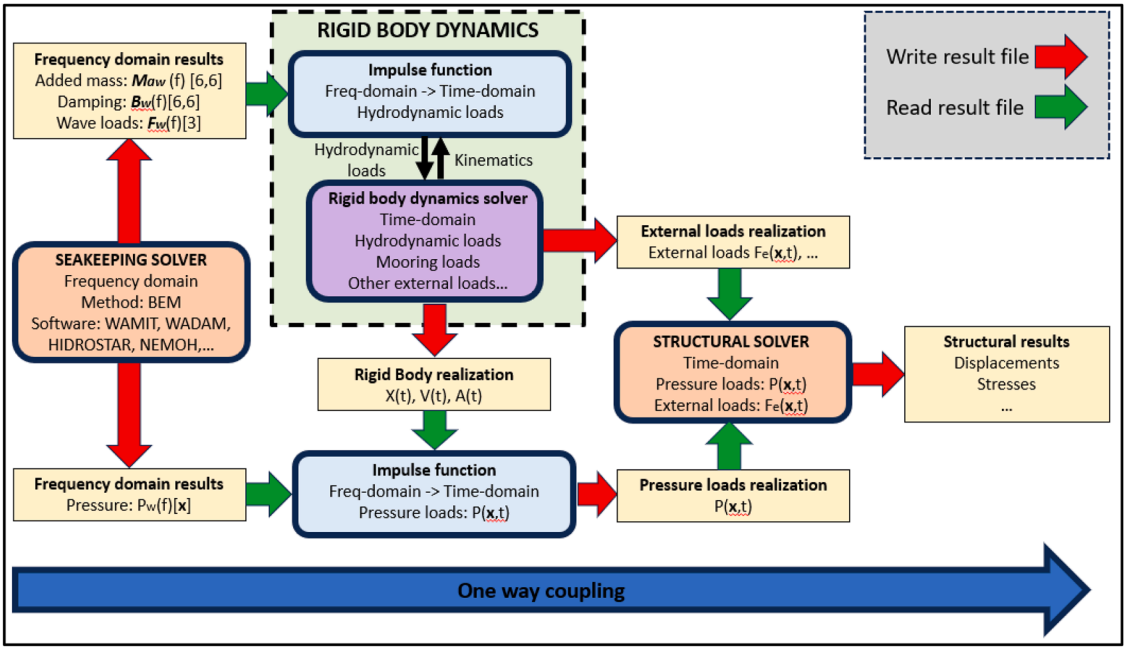

Fig. 1. Computational flow for hydroelastic analysis using current numerical tools.

- The approach involves coupling in only one direction, restricting its applicability to highly rigid structures where hydro-elastic effects can be safely disregarded.
- Structural dynamic simulations are a bottleneck for hydro-elastic analysis. Often a quasi-static approach is used to reduce computational times (hiding potential resonance/dynamic effects).

In this work, a different approach is taken (see Fig. 2). This is based on a computational framework where all external loads are simultaneously computed and applied, in the time-domain, to the structural system dynamics. The tightly coupled hydro-elastic problem is solved iteratively. It should be highlighted that the fact that both solvers are integrated within a single framework allows for direct memory communication between them, avoiding the need to exchange information through files.

The implementation of this methodology requires a time-domain approach and the efficient integration of hydro and elastic solvers. However, the computational resources needed to solve a fully coupled problem can be prohibitively high for practical applications.

In [35], the authors of this work analysed different strategies for coupling the seakeeping hydrodynamics and structural dynamics using solvers developed in house and integrated into the commercial packages SeaFEM [46] and RamSeries [47]. Both solvers are implemented under the same programming framework, allowing direct communication between them and the use of OpenMP for the parallel execution of both solvers. However, that work left open the question of how to reduce the significant computational resources required for those calculations.

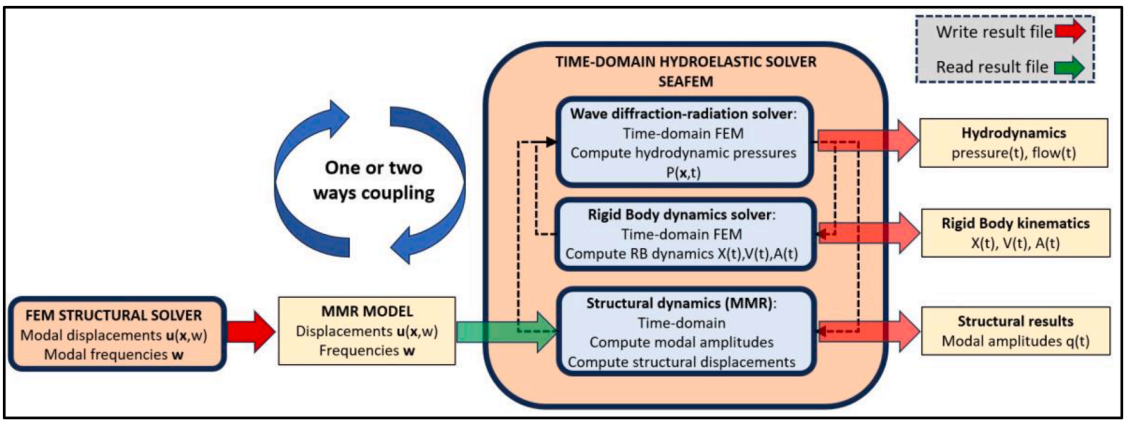

Fig. 2. Hydro-elastic computational framework.

It has been reported that most of the computational time required when coupling with potential flow hydrodynamics is taken to solve structural dynamics [35,48]. To overcome this bottleneck, the authors proposed a reduce order model based on modal matrix reduction in [45], where the number of degrees of freedom (DOF) for the structural problem can be largely reduced alongside its computational cost. However, the accuracy of this approach can be limited, especially in structural details, unless a large number of modes are used to capture the solution.

In this work a different approach is used to improve the reduce order model fidelity. First, the structural solver is used only to obtain structural particulars such as the modal base and material properties. Then, in a second stage, the seakeeping solver reads the structural particulars, building the structural dynamics equations coupled with the seakeeping hydrodynamics equations. This way, there is no need to execute the structural solver for each hydro-elastic execution with consequently an advantage in saving computational cost. Furthermore, to increase the accuracy of the reduced approach, this work proposes a combined methodology in which a residual FEM solution is computed alongside the reduced model, still achieving a substantial reduction in the overall computational effort required.

The numerical details of the developed computational hydro-elastic solver are provided below.

3. Hydro-elastic solver

3.1. Governing hydro-elasticity equations of motion

The general form of the governing equations for structural dynamics can be written as [35]:

$$\nabla \cdot \boldsymbol{\sigma} + \boldsymbol{b} = \rho \ddot{\boldsymbol{u}} \ \boldsymbol{in}\ \boldsymbol{\Omega_s}, \tag{1}$$

$$\boldsymbol{u} = \bar{\boldsymbol{u}} \quad \boldsymbol{on}\ \boldsymbol{P} \in \boldsymbol{S_u}, \tag{2}$$

$$\boldsymbol{\sigma} \cdot \boldsymbol{n} = \bar{\boldsymbol{t}} \quad \boldsymbol{on}\ \boldsymbol{P} \in \boldsymbol{S_\sigma}, \tag{3}$$

where $\boldsymbol{\sigma}$ is the stress tensor, $\boldsymbol{b}$ is the mass force vector, and Ω_s is the structural domain, $\boldsymbol{u}$ is the structural displacement vector field, S_u is the part of the structural external surface with prescribed displacements $\bar{\boldsymbol{u}}$, S_σ is the part of the structural external surface with prescribed tractions $\bar{\boldsymbol{t}}$. In the case of a fluid-structure problem, $\bar{\boldsymbol{t}}$ includes the dynamic fluid pressure field $\bar{\boldsymbol{f}}$ and other external loads.

The integral form of the above governing equations for a hydro-elasticity problem, modeled using the Finite Element Method (FEM), can be written in matrix form as [3]:

$$\bar{\bar{\boldsymbol{M}}}\ddot{\boldsymbol{U}} + \bar{\bar{\boldsymbol{B}}}\dot{\boldsymbol{U}} + \bar{\bar{\boldsymbol{K}}}\boldsymbol{U} = \boldsymbol{P} + \boldsymbol{F} + \boldsymbol{G}. \tag{4}$$

The matrixes $\bar{\bar{\boldsymbol{M}}}$, $\bar{\bar{\boldsymbol{B}}}$ and $\bar{\bar{\boldsymbol{K}}}$ represent the mass, damping and stiffness matrixes, respectively. $\boldsymbol{P}$, $\boldsymbol{F}$ and $\boldsymbol{G}$, are the column vectors of generalized forces associated with the loading. The fluid loading is simply represented by the generalized force vector $\boldsymbol{P}$, while $\boldsymbol{F}$ corresponds to concentrated loads (e.g., mooring or propulsion forces), and $\boldsymbol{G}$ represents generalized gravitational forces. Finally, $\boldsymbol{U}$ is the vector of nodal unknowns (displacements and rotations).

In the above equation, the static (e.g. hydrostatic and gravitational forces) and dynamic loads and displacements can be split as follows:

$$\boldsymbol{P}(\boldsymbol{t}) = \boldsymbol{P_D}(\boldsymbol{t}) + \boldsymbol{P_S}, \tag{5}$$

$$\boldsymbol{F}(\boldsymbol{t}) = \boldsymbol{F_D}(\boldsymbol{t}) + \boldsymbol{F_S}, \tag{6}$$

$$\boldsymbol{U}(t) = \boldsymbol{U}_D(t) + \boldsymbol{U}_S, \tag{7}$$

where D stands for dynamic and S for static. Then, the structural equations can be also split as:

$$\bar{\bar{\boldsymbol{M}}}\ddot{\boldsymbol{U}}_{\boldsymbol{D}} + \bar{\bar{\boldsymbol{B}}}\dot{\boldsymbol{U}}_{\boldsymbol{D}} + \bar{\bar{\boldsymbol{K}}}\boldsymbol{U_D} = \boldsymbol{P_D} + \boldsymbol{F_D}, \tag{8}$$

$$\bar{\bar{\boldsymbol{K}}}\ \boldsymbol{U_S} = \boldsymbol{P_S} + \boldsymbol{F_S} + \boldsymbol{G}, \tag{9}$$

where $\boldsymbol{P_S}$ represent the loads due to the hydrostatic pressure at equilibrium position, $\boldsymbol{F_S}$ the static concentrated loads such as pretension of mooring lines, and $\boldsymbol{G}$ corresponds to the self-weight. $\boldsymbol{P_D}$ represents the hydrodynamic component (seakeeping) of the fluid loads and $\boldsymbol{F_D}$ the dynamic component of the concentrated loads (e.g. propulsion forces). Eq. (9) only needs to be solved once, but the dynamic counterpart (8) requires solving the corresponding system of equations multiple times throughout the simulation. To reduce the required computational effort in solving Eq. (8), the Modal Matrix Reduction (MMR) technique is used [3,45,49]. The modal basis is obtained from the free vibration problem with no damping:

$$\left(\bar{\bar{\boldsymbol{M}}}^{-1}\bar{\bar{\boldsymbol{K}}}\right)\boldsymbol{D_i} = \boldsymbol{\Omega_i}^2\boldsymbol{D_i}, \tag{10}$$

The real and positive eigenvalues, Ω_i, are the natural frequencies and each is associated with a characteristic eigenvector or mode, $\boldsymbol{D}_i$. Without loss of generality [49], the structural displacements can be expressed as a linear combination of the eigenvectors:

$$\boldsymbol{U}_D(t) = \sum_{i=1}^{N_{DOF}} \boldsymbol{q}_i(t)\boldsymbol{D}_i, \tag{11}$$

where $\boldsymbol{Q} = \{q_i\}$ are the so-called modal generalized coordinates, and N_{DOF} is the number of degrees of freedom of the structural problem. It follows from this definition of $\boldsymbol{Q}$ that

$$\boldsymbol{U} = \bar{\boldsymbol{D}}\boldsymbol{Q}, \tag{12}$$

If this expression of $\boldsymbol{U}$ is substituted in the general equation of motion (8), and the equation is pre-multiplied by $\bar{\boldsymbol{D}}^T$, results that

$$\bar{\boldsymbol{A}}\ddot{\boldsymbol{Q}} + \bar{\boldsymbol{D}}^T\bar{\boldsymbol{B}}\bar{\boldsymbol{D}}\dot{\boldsymbol{Q}} + \bar{\boldsymbol{Z}}\boldsymbol{Q} = \bar{\boldsymbol{D}}^T\boldsymbol{P}_D + \bar{\boldsymbol{D}}^T\boldsymbol{F}_D, \tag{13}$$

where $\bar{\boldsymbol{A}}$, $\bar{\boldsymbol{Z}}$ are the diagonal generalized mass and stiffness matrixes that, according to the usual orthonormalization of the eigenvalues, are defined as

$$\bar{\boldsymbol{A}} = \begin{cases} a_{ij} = 1, \textit{for } i = j \\ a_{ij} = 0, \textit{for } i \neq j \end{cases} \quad \bar{\boldsymbol{Z}} = \begin{cases} z_{ij} = \Omega_i^2, \textit{for } i = j \\ z_{ij} = 0, \textit{for } i \neq j \end{cases}. \tag{14}$$

If the damping term is modelled as either Rayleigh or modal damping, Eq. (13) can be written as:

$$\ddot{\boldsymbol{q}}_i + c_i\dot{\boldsymbol{q}}_i + \Omega_i^2\boldsymbol{q}_i = (\boldsymbol{P}_D + \boldsymbol{F}_D)\cdot\boldsymbol{D}_i = \boldsymbol{h}_i(t), \quad i = 1, 2, \cdots, N_{DOF}. \tag{15}$$

$$c_i = \begin{cases} \alpha_M + \alpha_K\Omega_i^2 & \textit{Rayleigh} \\ 2\eta\Omega_i & \textit{Modal damping} \end{cases}, \tag{16}$$

where η represents the percentage respect to the critical modal damping.

So far, we have merely performed various manipulations to obtain an equation equivalent to the original equation of motion (8). The idea behind the MMR approach is that, generally, only the lower frequency modes are excited and needed to obtain an accurate approximation of the structural solution. Therefore,

$$\boldsymbol{U}_{MMR}(t) = \sum_{i=1}^{N_m} \boldsymbol{q}_i(t)\boldsymbol{D}_i \approx \boldsymbol{U}_D(t) \quad N_m \ll N_{DOF}. \tag{17}$$

To ensure that the selection of these modes is sufficient to accurately approximate the complete solution, it is common to use the criterion that the highest frequency of these modes, Ω_{N_m}, sufficiently exceeds the highest excitation frequency ω_{max} [49]:

$$\Omega_{N_m} \geq 4\cdot\omega_{max}. \tag{18}$$

If the body is unanchored and the stiffness matrix $\bar{\boldsymbol{K}}$ is positive semi-definite, Eq. (10) has six zero roots. Then, the modal generalized coordinates fall naturally in two groups $\boldsymbol{Q}_R$, $\boldsymbol{Q}_D$ [3], where:

$$\boldsymbol{Q}_R = \{\boldsymbol{q}_1, \boldsymbol{q}_2, \ldots, \boldsymbol{q}_6\}, \tag{19}$$

refers to the 'rigid body' modes, and

$$\boldsymbol{Q}_D = \{\boldsymbol{q}_7, \boldsymbol{q}_8, \ldots, \boldsymbol{q}_{N_m}\}. \tag{20}$$

refers to the 'flexible body' modes. Then, the matrix equation of motion (15) can be partitioned to give

$$\left\{\ddot{\boldsymbol{Q}}_R = \boldsymbol{H}_R, \right. \tag{21}$$

$$\left\{\ddot{\boldsymbol{Q}}_D + \underset{D}{\bar{\boldsymbol{C}}}\dot{\boldsymbol{Q}}_D + \underset{D}{\bar{\boldsymbol{Z}}}\boldsymbol{Q}_D = \boldsymbol{H}_D, \right. \tag{22}$$

being $\boldsymbol{H}_R = \{h_1, h_2, \ldots, h_6\}$, $\boldsymbol{H}_D = \{h_7, h_8, \ldots, h_{N_{DOF}}\}$, the vectors of generalized modal forces and $\bar{\boldsymbol{C}}_D$ the corresponding damping matrix. In this work, the time integration of eq. (21) is based on a Newmark method.

The equations corresponding to the first six modes above are equivalent to solving the rigid body dynamics equations associated with the dynamic forces. However, the full rigid body dynamics equations can be more conveniently expressed in their conventional form:

$$\bar{\bar{M}}_{RD}\ddot{U}_{RB} + \bar{\bar{B}}_{RB}\dot{U}_{RB} + \bar{\bar{K}}_{RB}U_{RB} = P_{RB} + F_{RB} + G_{RB}, \tag{23}$$

where $\bar{\bar{M}}_{RD}$, $\bar{\bar{B}}_{RB}$, and $\bar{\bar{K}}_{RB}$ are the mass, damping, and hydrostatic restoring matrices associated with the rigid body degrees of freedom; U_{RB} is the vector containing the three translational and three rotational components of the rigid body motion; and P_{RB}, F_{RB}, and G_{RB} are the vectors of integrated hydrodynamic, external (concentrated) and self-weight forces and moments acting on the body.

The elastic energy will be used to measure the fidelity of the MMR solution to approximate the full order FEM solution. The dynamic elastic energy of the full order FEM solution, $E^D(t)$, and that of the reduced order (MMR) solution, $E^D_{MMR}(t)$, can be calculated as:

$$E^D_{MMR}(t) = U_D^T \bar{\bar{K}} U_D, \tag{24}$$

$$E^D_{MMR}(t) = u^T_{MMR}\bar{\bar{K}}u_{MMR} = \sum_{i=1}^{i=N_m}\frac{1}{2}\Omega_i^2 q_i^2. \tag{25}$$

In order to integrate over time the structural dynamic equations, the second-order implicit Newmark scheme with γ=0.5 and β=0.5 is used for both, the full order FEM and MMR models. In this work, the seakeeping loads P_D are calculated in time-domain with a wave diffraction-radiation solver based on the Finite Element Method, as presented below.

3.1.1. Strong FEM acceleration with MMR

As previously noted, when MMR is applied with a limited number of modes, the accuracy can degrade, especially in capturing structural details. To overcome this drawback, this work proposes a combined methodology in which a residual FEM solution is computed alongside the reduced model, still achieving a reduction in the overall computational effort required.

It was shown in [49] that those modes with modal frequency larger than four times the frequency of the structural loads respond in quasistatic regime, while for modes with modal frequencies lower respond in the dynamic regime. Based on the previous idea, the dynamic response of the structure can be computed using the strong coupling with an MMR base such that:

$$\ddot{q}_i + c_i\dot{q}_i + \Omega_i^2 q_i = a_i \cdot \sum f_D^j \sin\left(\Omega_j^{load} t + \chi_j\right),\ i = 1,\ldots N_L\ \Omega_i < 4\Omega_j^{load}, \tag{26}$$

$$U_{MMR}(t) = \sum_{i=1}^{N_m} q_i(t) D_i, \tag{27}$$

where N_L is the number of modes with modal frequency lower than a threshold frequency in the order of four times the frequency loads, and χ_j the phase load. On the other hand, the orthogonal component to u^L_{MMR} of the solution could be computed by using the weak coupling and solving the residual system:

$$\bar{\bar{S}}U_D^* = P_D + F_D - \bar{\bar{S}}U_{MMR}, \tag{28}$$

$$U_D = U_{MMR} + U_D^*, \tag{29}$$

where $\bar{\bar{S}}$ represents the resulting structural system of equations using the FEM.

This way, for a strong coupled simulation, instead of solving the full order FEM system for each iteration within each time step, the MMR is used to compute the strongly coupled dynamic response, while the residual FEM system is only solved once per time step using the weak coupling once the dynamic component has converged within the current time step.

3.2. Seakeeping solver with forward speed (SeaFEM)

The seakeeping model with forward speed used in this work is a time-domain wave diffraction-radiation solver based on the FEM, developed in-house and integrated in the commercial framework SeaFEM [46]. The mathematical and numerical models implemented in SeaFEM have been extensively verified and validated. These can be found in [35,45,38–44].

Using a frame of reference where the OZ axis represents the vertical direction and whose origin is located at the free surface, the governing equations are given by [39]:

$$\Delta\varphi = 0, \quad in\ \Omega, \tag{30}$$

$$\partial_t\xi + (U + \nabla_h\varphi)\cdot\nabla_h\xi - \partial_z\varphi = 0, \quad on\ z = 0\,, \tag{31}$$

$$\partial_t\varphi + U\cdot\nabla_h\varphi + \frac{1}{2}\nabla_h\varphi\cdot\nabla_h\varphi + g\xi = 0, \quad on\ z = 0, \tag{32}$$

$$v_\varphi \cdot n_p = (v_p - U)\cdot n_p, \quad on\ P \in \Gamma_B, \tag{33}$$

$$P_p = -\rho g\left(z_p + r_{pz}\right) - \rho\left(\frac{\partial \varphi}{\partial t} + \boldsymbol{U}\cdot\nabla\varphi + \frac{1}{2}\nabla\varphi\cdot\nabla\varphi\right), \tag{34}$$

where φ is the velocity potential ($\boldsymbol{v}_\varphi = \nabla\varphi$), ξ is the free surface elevation, Ω is the fluid domain, $z = 0$ represents the still water level, Γ_B is the wetted Surface of a floating body, $\boldsymbol{n}_p$ is a normal vector to a Surface at point P, $\boldsymbol{v}_p$ is the velocity of point p, z_p is the initial vertical position of point P, ∇_h is the gradient operator in the horizontal directions, and r_{pz} is the vertical displacement of P. The solution can be split into the incident and diffracted-radiated wave components:

$$\varphi = \psi + \phi, \tag{35}$$

$$\xi = \zeta + \eta, \tag{36}$$

where ψ and ζ are the velocity potential and wave elevation respectively for the incident wave field, and ϕ and η are the velocity potential and free surface elevation respectively for the diffracted-radiated waves respectively. The incident wave field is described by the Airy wave analytical solution. Introducing the separation of variables into the governing equations, the wave diffraction-radiation problem is obtained in terms of ϕ and η as independent variables.

In this work, double body linearization is used. Double body linearization assumes that $\nabla_h\,\phi \sim O(1)$, but it can be split into two terms: $\nabla_h\,\phi = \nabla_h\phi^{DB} + \nabla_h\phi^{*}$, where $\nabla_h\phi^{DB}$ represents the flow field when the free surface is substituted by a wall (equivalent to a symmetric case using a double body). Then $\nabla_h\,\phi$ is approximated as $\nabla_h\phi^{DB}$ perturbed by $\nabla_h\phi^{*}$, which means $\nabla_h\phi^{DB} \sim O(1)$ and $\nabla_h\phi^{*} \sim \mathrm{O}(\epsilon)$. Then the first-order free surface boundary conditions become:

$$\frac{\partial \phi}{\partial t} + \left(\boldsymbol{U} + \nabla_h\,\phi^{DB}\right)\cdot\nabla_h\phi - \frac{1}{2}\nabla_h\,\phi^{DB}\,\nabla_h\,\phi^{DB} + \nabla_h\,\phi^{DB}\cdot\nabla_h\,\psi + \frac{P_{fs}}{\rho} + g\eta = 0, \tag{37}$$

$$\frac{\partial \eta}{\partial t} + \left(\boldsymbol{U} + \nabla_h\,\phi^{DB}\right)\cdot\nabla_h\,\eta + \nabla_h\,\phi^{DB}\cdot\nabla_h\,\zeta - \partial\phi\Big/\partial z = 0, \tag{38}$$

and the pressure induced at point P is:

$$P_p = -\rho\left(\frac{\partial \phi}{\partial t} + \left(U_b + \nabla_h\phi^{DB}\right)\cdot\nabla_h\,\phi - \frac{1}{2}\nabla_h\phi^{DB}\,\nabla_h\phi^{DB} + \nabla_h\phi^{DB}\cdot\nabla_h\,\psi\right). \tag{39}$$

More details on the wave diffraction-radiation governing equations can be found in [39].

As stated above, the FEM will be used to obtain the numerical solution of the above system. The SUPG (Streamline Upstream Petrov-Galerkin) scheme is used for the integration of the free surface kinematic and dynamic boundary conditions. The resulting system of equations in matrix form, can be written as [39,43]:

$$\bar{\bar{\boldsymbol{L}}}\boldsymbol{\Phi} = \boldsymbol{\Theta}_B + \boldsymbol{\Theta}_{TS} + \boldsymbol{\Theta}_R + \boldsymbol{\Theta}_{Z_0}, \tag{40}$$

where $\bar{\bar{\boldsymbol{L}}}$ is the Laplacian Matrix, and $\boldsymbol{\Theta}_B$, $\boldsymbol{\Theta}_{TS}$, $\boldsymbol{\Theta}_R$, and $\boldsymbol{\Theta}_{Z_0}$, are the vectors resulting of integrating the body, transom stern, radiation, and free surface boundary condition respectively. $\boldsymbol{\Theta}_B$ is built from the velocity obtained by integrating eqs. (22) and (23).

The numerical details of this solver, as well as a number of verification and validation cases, can be found in [38,43].

3.2.1. Transom stern modelling

In the case of ships with transom sterns, the flow detaches from the lower edge of the transom, making the immersed surface of the transom to be dry. If the body boundary condition is still applied, it results in an unstable flow at the stern since the potential flow equations cannot predict the flow detachment at the transom edge. Hence, the flow detachment must be imposed by modifying the boundary conditions at the transom.

Fig. 3 sketches the transom stern boundary conditions imposed. To induce the flow detachment, a flow condition is imposed at the transom surface (Eq. (42)), and the free surface elevation is imposed to match the vertical position of the transom edge (Eq. (43)). Also, as the transom surface is dry, the free surface reference pressure is imposed (Eq. (44)), and so is the corresponding the pressure field:

$$\frac{1}{2}\boldsymbol{U}_{TS}^2 + gZ_{TS} = \frac{1}{2}\boldsymbol{U}_{\infty}^2, \tag{41}$$

$$\left(\boldsymbol{U} + \boldsymbol{v}_\varphi\right)\cdot\boldsymbol{n}_{TS} = \boldsymbol{U}_{TS}\cdot\boldsymbol{n}_{TS}, \quad on\ P \in \Gamma_{TS}\,, \tag{42}$$

$$\xi_{\mathrm{P}_0} = \mathrm{Z}_{\mathrm{TS}}, \quad \text{on } \mathrm{P}_0 \in \Gamma_{\mathrm{TS}} \cap \{\mathrm{z} = 0\}\,, \tag{43}$$

$$P_P = 0, \quad on\ P \in \Gamma_{TS}, \tag{44}$$

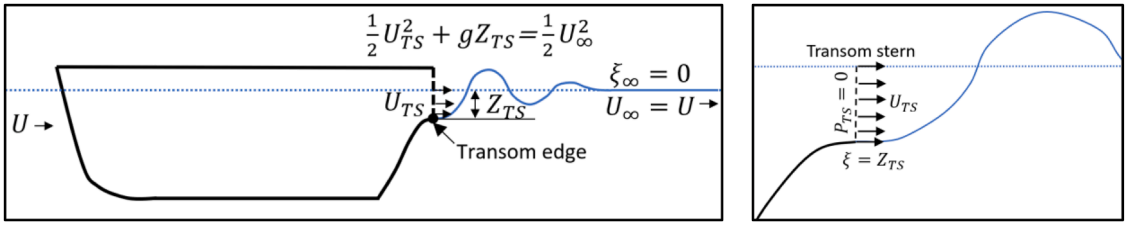

Fig. 3. Transom stern boundary condition.

3.3. Fluid-structure interaction

The fluid-structure interaction approach is illustrated in Fig. 4. In this work, a partitioned tightly coupled (two ways) approach is used [35]. Once Eq. (40) is solved, the pressure of the structure boundary is calculated using Eq. (39) and integrating to obtain $\boldsymbol{P_D}$. Then, eqs. (21)-(22) are solved to obtain the displacement of the structure that allows computing $\boldsymbol{\Phi}_{\Gamma_B}$. The tightly coupled approach is based on an iterative process in which the coupling variables are interpolated back and forth between the fluid and structural domains at the common body boundary, Γ_B. Besides the tightly coupled approach, a one-way weak coupling -where the effect of the structural deformation on the fluid is neglected- will also be analyzed in this work. Fig. 4 illustrates the concept of how pressure-displacement information is transferred across the fluid-structure common boundary Γ_B.

As mentioned above, the seakeeping and structural problems will be discretized using the FEM. However, it is not required to use identical discretization for the common boundary Γ_B where the interaction occurs. Spatial linear interpolators have been used in this work to transfer the fluid pressure to the structure boundary and to transfer the structural displacements to the fluid boundary.

$$\boldsymbol{P}_{S,\Gamma_B} = \overset{=F\to S}{\boldsymbol{I}}\, \boldsymbol{P}_{F,\Gamma_B}, \tag{45}$$

$$\boldsymbol{U}_{F,\Gamma_B} = \overset{=S\to F}{\boldsymbol{I}}\, \boldsymbol{U}_{S,\Gamma_B}. \tag{46}$$

where $\mathbf{P}_{S,\Gamma_B}\boldsymbol{U}_{S,\Gamma_B}$, $\mathbf{P}_{F,\Gamma_B}$, and $\boldsymbol{U}_{F,\Gamma_B}$ are the fluid pressure and structural displacements at the structural and fluid discretization over Γ_B respectively, and $\overset{=F\to S}{\boldsymbol{I}}$ and $\overset{=S\to F}{\boldsymbol{I}}$ are the corresponding interpolation matrices.

Based on all the above, the formulation of the complete problem can be written as follows. Let us consider a uniform partition of the time interval of analysis $[0, T]$, with time step size dt. A double superscript n,j will be used to indicate the time step n at which the

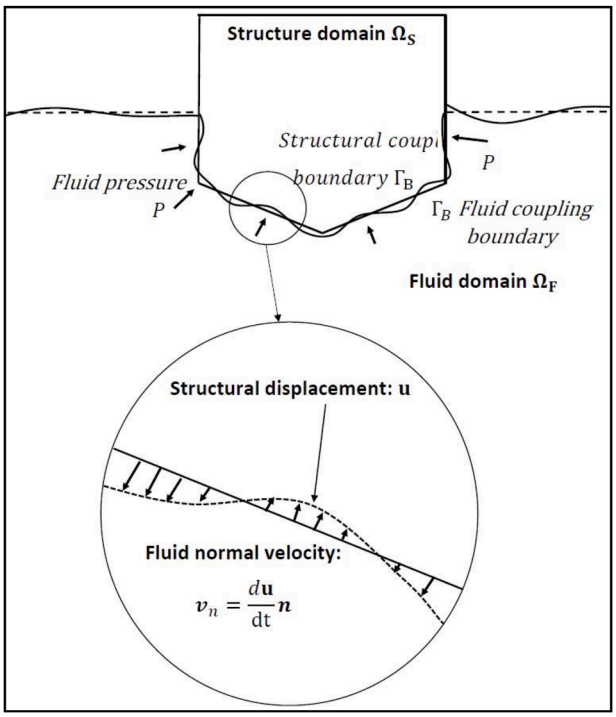

Fig. 4. Fluid-structure interaction concept.

solution is computed, and the iteration index j. The statement of the discrete tightly coupled iterative partitioned formulation consists of finding $\boldsymbol{U}_S$, $\boldsymbol{U}_D^{n+1}$, $\boldsymbol{U}_{RB}^{n+1}$ and $\boldsymbol{\Phi}^{n+1}$ as the solution of the following problem:

Solve the static structural equations (step 0)

$$\bar{\bar{\boldsymbol{K}}}\,\boldsymbol{U}_S = \boldsymbol{P}_S + \boldsymbol{F}_S + \boldsymbol{G}. \tag{47}$$

Solve the structural dynamics equations of motion (step n, iteration i)

$$\underset{D}{\ddot{\boldsymbol{Q}}}^{n+1,i} + \bar{\bar{\boldsymbol{C}}}_D \dot{\boldsymbol{Q}}_D^{n+1,i} + \bar{\bar{\boldsymbol{Z}}}_D \boldsymbol{Q}_D^{n+1,i} = \boldsymbol{H}_R{}^{n+1,i}, \tag{48}$$

$$\boldsymbol{U}_D^{n+1,i} = \bar{\bar{\boldsymbol{D}}}_D \boldsymbol{Q}_D. \tag{49}$$

Calculate the structural velocity on fluid boundary Γ_{Bf} (step n, iteration i)

$$\boldsymbol{U}_{\Gamma_{Bf}}^{n+1,i} = \bar{\bar{\boldsymbol{I}}}^{S\to F} \left[\boldsymbol{U}_R^{n+1,i} + \boldsymbol{U}_D^{n+1,i}\right]_{\Gamma_{Bs}}, \tag{50}$$

$$\boldsymbol{\Theta}_{\Gamma_{Bf}}^{n+1,i} = \mathrm{N}_{\Gamma_{Bf}} \left[\dot{\boldsymbol{U}}_{\Gamma_{Bf}}^{n+1,i} + \mathscr{E}_{\Gamma_{Bf}}\left(\dot{\boldsymbol{U}}_{RB}^{n+1,i-1}\right)\right]. \tag{51}$$

Solve the seakeeping governing equations *(step n, iteration i)*

$$\bar{\bar{\boldsymbol{L}}}\boldsymbol{\Phi}^{n+1,i} = \boldsymbol{\Theta}_B^{n+1,i} + \boldsymbol{\Theta}_{TS}^{n+1,i} + \boldsymbol{\Theta}_R^{n+1,i} + \boldsymbol{\Theta}_{Z_0}^{n+1,i}\boldsymbol{\Theta}_{Z_0}, \tag{52}$$

$$\boldsymbol{P}_{\Gamma_{Bf}}^{n+1,i} = \Gamma\left[\dot{\Phi}_{\Gamma_{Bf}}^{n+1,i}, \Phi_{\Gamma_{Bf}}^{n+1,i}\right]. \tag{53}$$

Solve the rigid body dynamics equations *(step n, iteration i)*

$$\boldsymbol{P}_{RB}^{n+1,i} = \mathrm{N}_{RB}\boldsymbol{P}_{\Gamma_{Bf}}^{n+1,i}, \tag{54}$$

$$\bar{\bar{\boldsymbol{M}}}_{RD}\dot{\boldsymbol{U}}_{RB}^{n+1,i} + \bar{\bar{\boldsymbol{B}}}_{RB}\dot{\boldsymbol{U}}_{RB}^{n+1,i} + \bar{\bar{\boldsymbol{K}}}_{RB}\boldsymbol{U}_{RB}^{n+1,i} = \boldsymbol{P}_{RB}^{n+1,i} + \boldsymbol{F}_{RB}^{n+1,i} + \boldsymbol{G}_{RB}^{n+1,i}. \tag{55}$$

Transfer the fluid pressure to the structural boundary Γ_{Bf} (step n, iteration i)

$$\boldsymbol{P}_{\Gamma_{Bs}}^{n+1,i+1} = \bar{\bar{\boldsymbol{I}}}^{F\to S}\boldsymbol{P}_{\Gamma_{Bf}}^{n+1,i}, \tag{56}$$

$$\boldsymbol{P}_D^{n+1,i+1} = \mathscr{E}_{\mathscr{D}}\left(\boldsymbol{P}_{\Gamma_{Bf}}^{n+1,i+1}\right), \tag{57}$$

$$\boldsymbol{H}_D^{n+1,i+1} = \underset{D}{\bar{\bar{\boldsymbol{D}}}}^{\boldsymbol{T}}\left[\boldsymbol{P}_D^{n+1,i+1} + \boldsymbol{F}_D^{n+1,i+1}\right]. \tag{58}$$

Static correction of the FEM solution (once converged in the time step)

$$\bar{\bar{\boldsymbol{S}}}\boldsymbol{U}_D^{*} = \boldsymbol{P}_D + \boldsymbol{F}_D - \bar{\bar{\boldsymbol{S}}}\boldsymbol{U}_D^{n+1,i}, \tag{59}$$

$$\boldsymbol{U}_D^{n+1} = \boldsymbol{U}_D^{n+1,i} + \boldsymbol{U}_D^{*}. \tag{60}$$

In the above, the subscripts Γ_{Bf} and Γ_{Bs} refers to the fluid and structure coupling boundaries.

As mentioned above, the iterative process allows for weak (one-way dynamic) coupling, and strong (two-ways dynamic) coupling. In the weak approach, the step corresponding to the calculation of the structural velocity on the fluid boundary Γ_{Bf} is omitted. In order to improve the stability and accelerate the convergence of the iterative scheme, the modified Aitkenś method [50] was implemented.

When using the 2-ways (strong) hydroelastic coupling, the convergence criteria used are:

- MMR coupling:

$$\epsilon_{MMR} = Max_i\left|\frac{q_i^k - q_i^{k-1}}{q_i^k}\right| < 10^{-5}\ i = 1, 2, \cdots,\ \textit{Number of modes}. \tag{61}$$

- Full order FEM coupling:

$$\epsilon_{FEM} = Max_i\left|\frac{\sum_{i=1}^{NDOF}\left(u_i^k - u_i^{k-1}\right)^2}{\sum_{i1}^{NDOF}\left(u_i^k\right)^2}\right| < 10^{-5}\ , \tag{62}$$

where k is the k-th iteration within the time step.

4. Discussion on the developed computational framework

As presented in the previous sections, the implemented computational framework allows all external loads to be simultaneously computed and applied in the time domain, with the fully hydro-elastic problem solved iteratively. It is important to note that, as shown in Fig. 2, the structural analysis tool is used offline to compute the structural system details (FEM system matrices and/or modes and model frequencies) and this information is then transferred to the computational framework. This enables the same computational framework to solve the coupled problems using the full order FEM approach, the reduced order MMR technique, or the hybrid method based on the static correction presented above. The strategy drawn in Fig. 2 has a number of advantages over the conventional one in Fig. 1:

- Reduces the number of interactions between different computational tools.
- Reduces the number of files to be written and read.
- Allows for strong coupling (important to account for flexibility).
- The structural output files are largely reduced in size $O\left(\frac{N_m}{N_{DOF}}\right)$.
- All structural external loads are computed simultaneously in each step and straightforwardly mapped onto the structural domain.
- Communication among solvers happens at RAM memory level, minimizing the communication overheads compared to partitioned coupled strategies based on independents software.

When computing a large number of long structural dynamics realizations, the need to write the time-series of the stresses leads to the problem of storing high number of result files. These files can be large in memory size, which is not only memory demanding, but computationally demanding in terms of reading and writing tasks.

The use of the MMR largely reduces the structural output file size since only the time-series of the modal amplitudes are reported. From these, several off-line computations can be performed for the structural assessment:

- Ultimate load analysis:
  - The structural energy can be quickly computed to identify those instants with maximum structural energy using Eq. (25).
  - Structural displacement field reconstruction using Eq. (11) for identified extreme instants.
  - Structural stresses computation from structural displacements.
  - Identification of hotspots.
- Fatigue damage analysis:
  - Hotspots identification.
  - Time-series structural displacement and stresses reconstruction using Eq. (11) at hotspots' readout elements.
  - Time-series structural stresses computation from structural displacements at hotspots' readout points.
  - Fatigue damage computation from structural stresses time-series at hotspots.

Furthermore, for many load-cases where the external loads can be assumed to be induced by linear waves, this framework allows to pre-compute modal response amplitude operators [MRAOs] [45]. Then, once MRAOs are known, it is straight forward to carry out dynamic realizations under irregular loads scenarios. This can largely further reduce the computational times enabling its use for fatigue damage computation and operational conditions like in a digital twin.

5. Application example

5.1. Ship description

Fig. 5 shows the structure of the ship used in this work as a case study to demonstrate the capabilities of the developed methodology presented here. The original structural FEM model was created in Maestro and imported into Ansys for processing and for generating the input files required by the hydroelastic computational analysis framework. The ship will be assumed to be navigating at a forward speed, and it has a transom stern. Table 1 provides the particulars of the ship.

Heave, roll and pitch natural periods have been obtained by simulation of free decay tests in still water. And viscous damping for heave, roll and pitch motions has been estimated as 5 % of the critical damping. Table 2 reports the natural periods and viscous damping.

The structural mesh used in this work (see Fig. 5) is composed of 30,137 shell elements and 12,105 beam elements. The shell element consists of 3D 3 or 4 node shell, depending on whether it is a triangular or quadrilateral element, and 9 or 12 integration points. Integration points are divided into 3 or 4 in-plane and 3 layers through the thickness. Table 3 provides the overall particulars of the structural FEM mesh, as well as the total number of DOF.

The seakeeping computational domain consists of an unstructured mesh with 749,391 tetrahedral elements and 138,169 nodes. Minimum (near field) FE size is 0.15 m and maximum (far field) is 10 m. Fig. 6 shows the SeaFEM meshes used. The time step used in the simulations is 0.05 s.

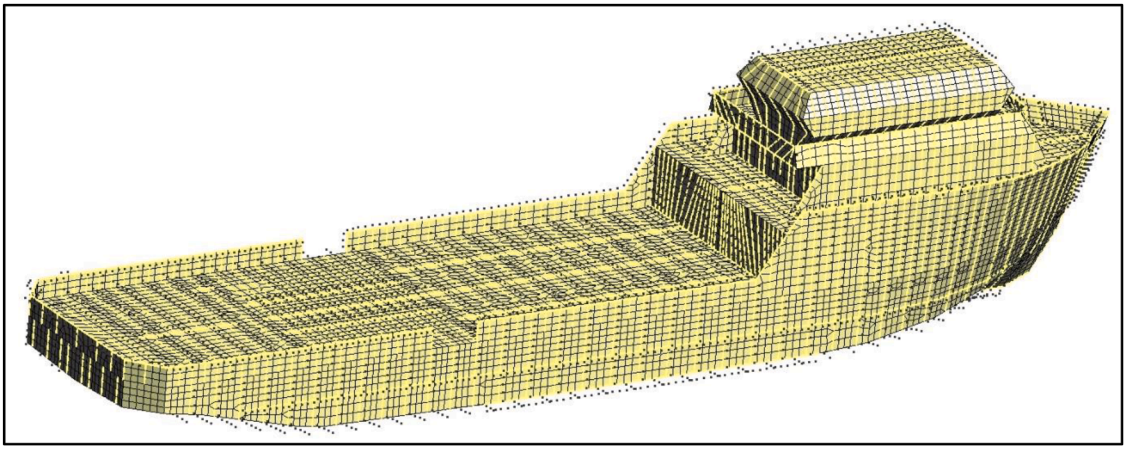

Fig. 5. 3D Ansys mesh.

Table 1
Ships particulars.

Mass/Displacement	1153 t
Overall Length	50.290 m
Overall Beam	11.030 m
Draft	3.060 m
Longitudinal distance of gravity centre (X_G)	23.345 m
Vertical distance of gravity centre (Z_G)	−0.395 m
Longitudinal distance of buoyancy centre (X_B)	23.320 m
Vertical distance of buoyancy centre (Z_B)	−1.260 m
Roll radii of inertia (r_{xx})	4.004 m
Pitch radii of inertia (r_{yy})	13.172 m
Yaw radii of inertia (r_{zz})	13.290 m
Roll-Yaw radii of inertia (r_{xz})	−3.935 m

Table 2
Rigid body natural periods and viscous damping.

Heave natural period (T_{heave})	4.7 s
Roll natural period (T_{roll})	5.37 s
Pitch natural period (T_{pitch})	4.5 s
$C_{heave} = 2 \cdot 0.05 \cdot Mass \cdot (2\pi / T_{heave})$	154,14 KN/(m s^{-1})
$C_{roll} = 2 \cdot 0.05 \cdot Mass \cdot r_{xx}^2 \cdot (2\pi / T_{roll})$	2147.73 KN·m/(rad s^{-1})
$C_{pitch} = 2 \cdot 0.05 \cdot Mass \cdot r_{yy}^2 \cdot (2\pi / T_{pitch})$	27,796.33 KN·m/(rad s^{-1})

6. Comparison of transom stern modelling

To assess the accuracy of the boundary conditions applied at the transom stern in reproducing the wave elevation and pressure field, a comparative analysis is conducted on the vessel under study. The evaluation considers two configurations: one with the stern boundary condition imposed and one without it. Fig. 7 and Fig. 8 show the free surface elevation and dynamic pressure field for the ship analysed in this work when navigating at 10 knots in still waters. It is observed that when the transom conditions are not applied, the free surface elevation at the stern is unrealistic.

Table 3
Structural Mesh particulars.

Number of FE elements	42,242
Number of nodes	39,186
Number of DOF	235,116

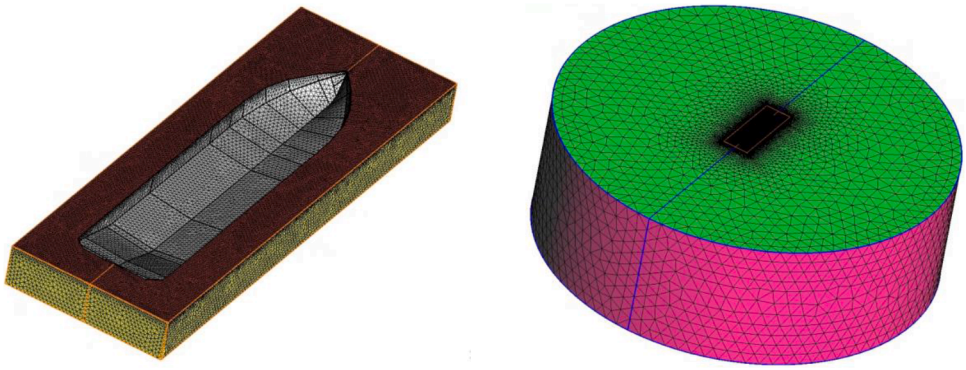

Fig. 6. SeaFEM Finite Element mesh left: Nearfield mesh; right: full computational domain mesh.

6.1. *Modal frequency and damping in floating conditions*

The structural response is largely influenced by the first modes of the ship. Hence, the natural frequencies of the lower frequency modes are critical for structural dynamics. In this section, the hydro-elastic model based on MMR is used to evaluate the change in the modal frequency of the lower modes in floating conditions with respect to dry conditions. Also, the damping induced by the wave radiation is estimated.

The MMR technique [45] starts with a modal analysis of the FEM structural model. A modal basis of 10,000 modes with no restrictions has been computed. The resulting modal frequencies are in a range from 4.55 Hz to 68.31 Hz. The first 6 elastic modes are shown in Fig. 9 including their "dry" modal frequencies. The first corresponds to the first bending mode.

When the ship is deployed in water, the structural displacements radiate waves (inducing fluid dynamic pressure) and cause a variation in the hydrostatic pressure. This implies changes in the modal frequency and introduces modal damping.

To quantify the effects of structural wave radiation, an extinction test analysis is performed for the first elastic modes assuming there is no structural damping. This test is carried out using the strong coupling described earlier. The ship is in hydrostatic equilibrium condition (subject to self-weight and hydrostatic pressure). The rigid body motions are kept fixed and one elastic mode at a time is set free. Then its modal amplitudes will evolve until it reaches equilibrium. Fig. 10 left shows the time evolution of the modal amplitude

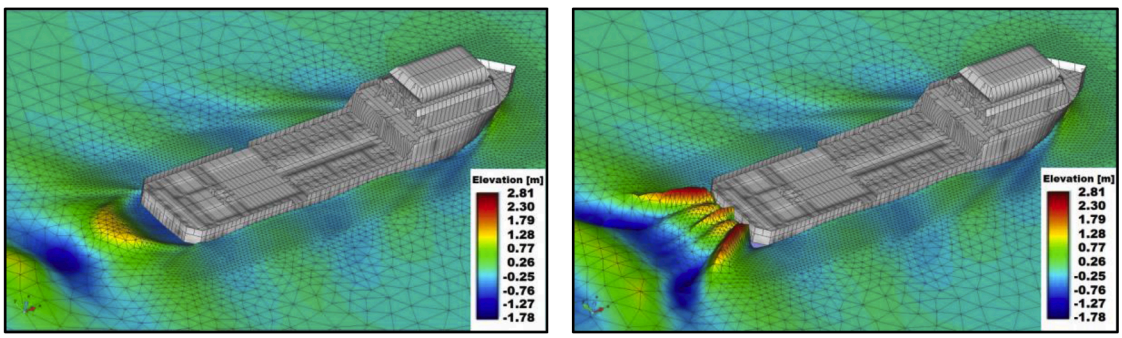

Fig. 7. Stern free surface elevation at $v = 10$kn Left: with transom stern conditions; Right: without transom stern conditions.

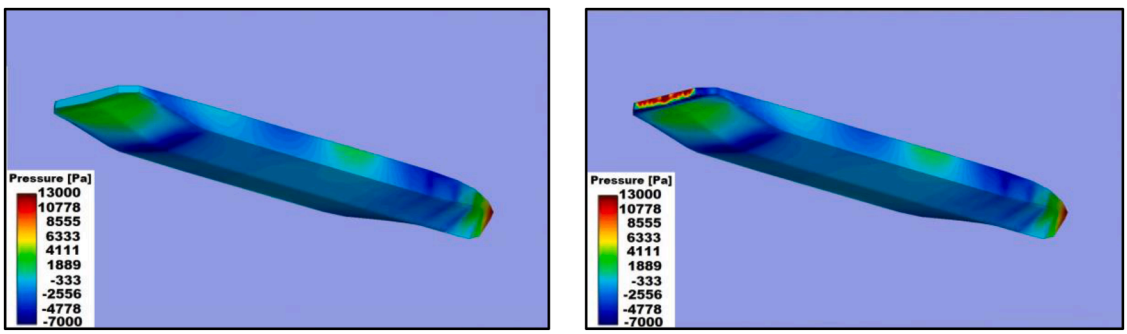

Fig. 8. Dynamic pressure fills at $v = 10$kn Left: with transom stern conditions; Right: without transom stern conditions.

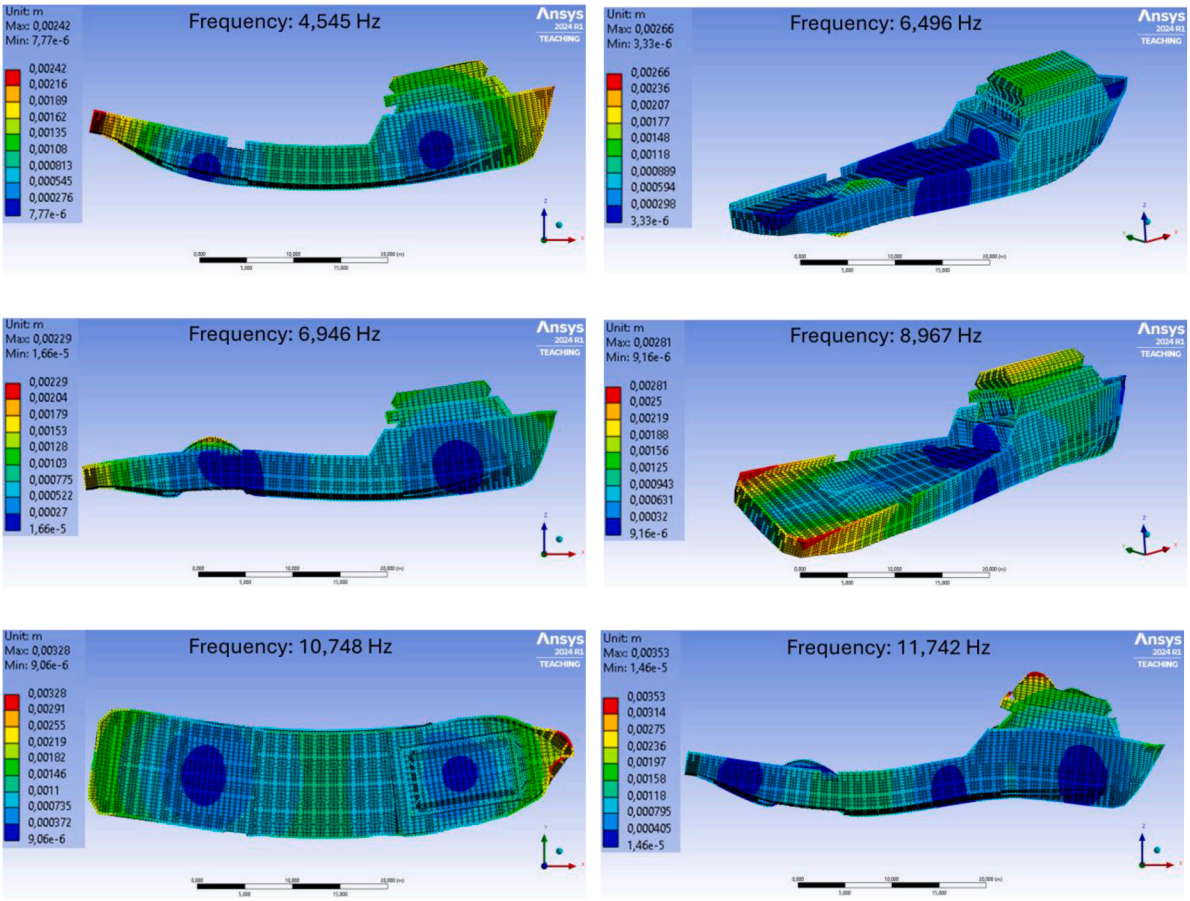

Fig. 9. First elastic dry modes. Color fill represents structural displacements.

for the first elastic mode. *Fig. 10* right shows a snapshot of the waves radiated during the extinction test.

Table 4 provides a change in the modal periods for the first five elastic modes. The damping is given as a percentage of the critical modal damping. It is observed that a significant change in the modal periods, while damping due to radiation, is quite small.

6.2. *Hydrostatic equilibrium*

The Reduced Order Model (ROM) using MMR is applied and compared to the Full Order Model (FOM) for the static case in which the ship is subject only to hydrostatic pressure and self-weight. The static FOM solution is obtained using the Mass and Stiffness matrices exported from the Ansys structural model, and the MMR is based on the modal basis exported from the Ansys structural model as well.

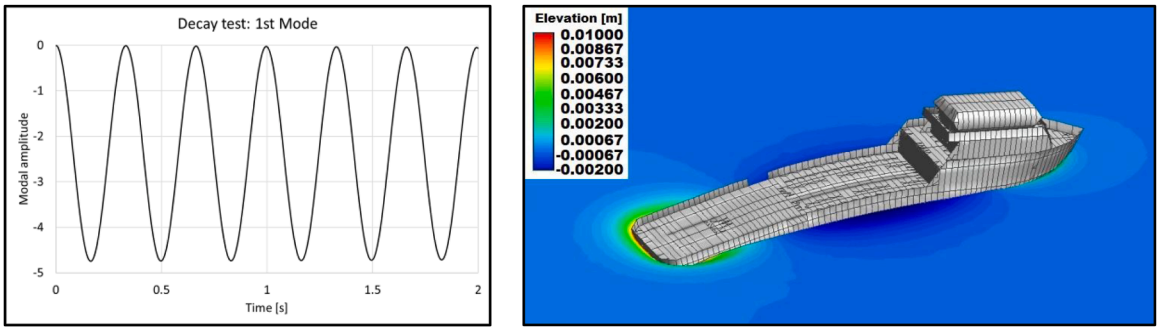

Fig. 10. Left: Extinction test for the first elastic mode. Right: Snapshot of deformed structure (amplified) and radiated waves (colour fill).

Table 4
Modal periods and damping for the first six elastic modes.

	1st Mode	2nd Mode	3rd Mode	4th Mode	5th Mode	6th Mode
Dry period [s]	0.220	0.154	0.144	0.112	0.093	0.085
Wet period [s]	0.332	0.171	0.188	0.136	0.104	0.120
Wave radiation damping [%]	0.063	0.124	0.232	0.370	0.377	0.730

Table 5 compares the maximum structural displacements and the structural energy. Fig. 11Fig. 1 shows the structural displacements computed using the FOM and the ROM with 10,000 modes. The ROM retains 99.7 % of structural energy compared with the FOM.

Fig. 12 left shows how energy is distributed across modes. It is observed how the first and third modes are dominant as expected. Fig. 12 right shows how much energy is recovered as the number of modes increases. Table 6 reports the number of modes needed to recover a percentage of energy with respect to the FOM solution. To recover 99 % of the energy, the first 3939 modes are needed. This implies a reduction in the number from 235,116 to 3939 which represents a reduction of 98.32 %.

6.3. Modal response amplitude operators (MRAOs) in head waves

In this section, MRAOs are computed in different regular head waves with a forward speed of 10 knots. They are computed using weak, quasistatic, and strong coupling. The quasistatic coupling is commonly used for structural analysis of marine structure, and it assumes that the frequency of the excitation loads is much lower than the modal frequencies. Hence the inertial and damping terms in eq. (8) are neglected, and the quasistatic response can be computed for any time instant by solving the system:

Table 5
Comparison of maximum and minimum structural displacements, and structural energy.

	Maximum (mm)	Structural Energy (J)
FOM	6.5844	6,424.02
ROM 10,000	6.5919	6,404.00

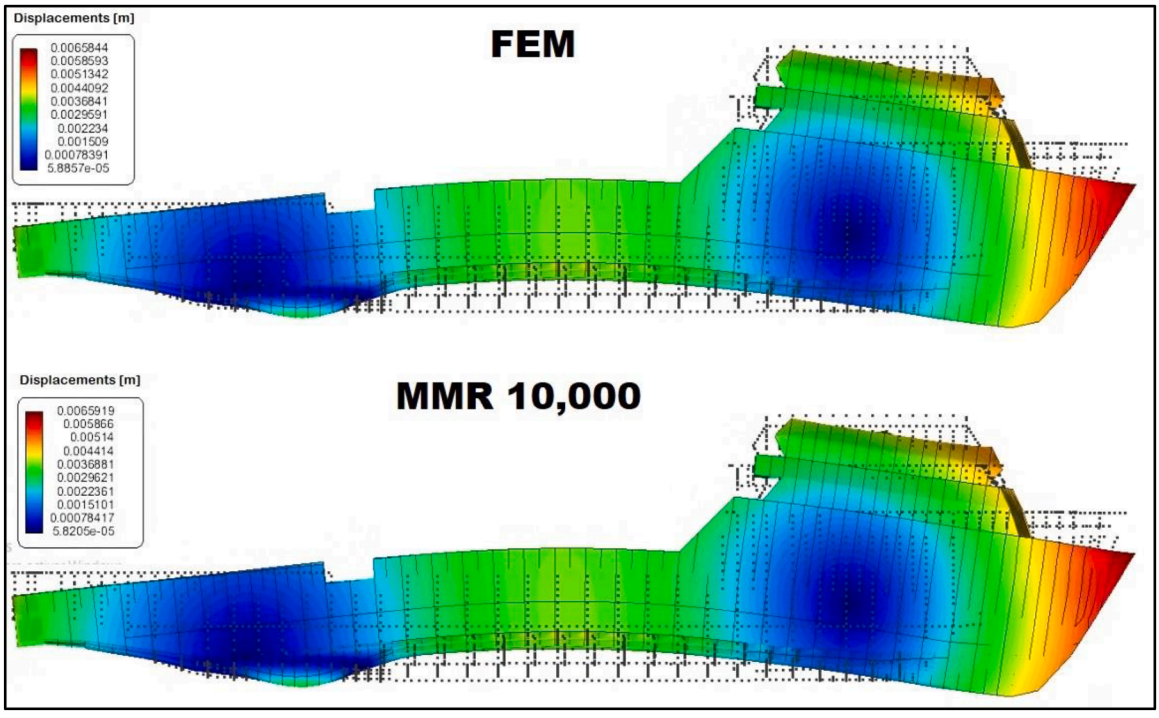

Fig. 11. Comparison of structural displacements (colour fill) in hydrostatic equilibrium condition.

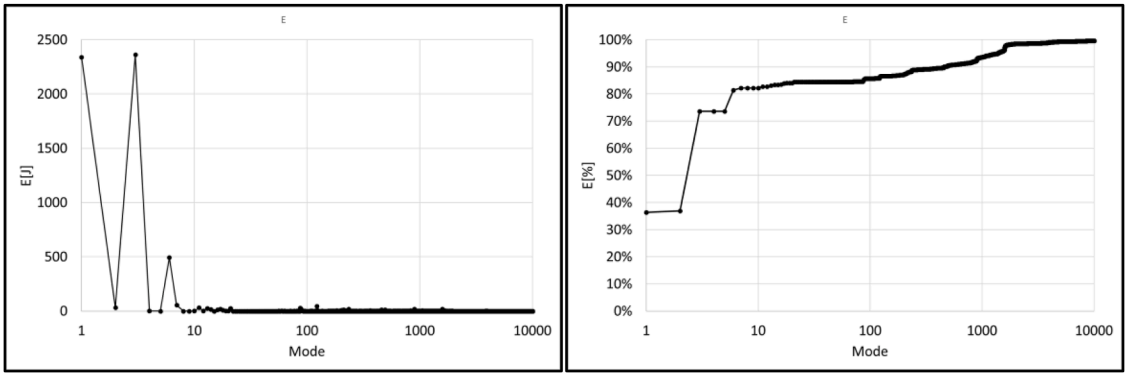

Fig. 12. Left: Modal energy distribution across modes; Right: Percentage of cumulative energy respect to FEM.

Table 6
Energy recovered vs Number of modes.

E [%]	80	90	95	99
Number of modes	6	456	1383	3939

$$\overline{\overline{\boldsymbol{K}}}\,\boldsymbol{U}_D^{qs} = \boldsymbol{P}_D + \boldsymbol{F}_D, \tag{61a}$$

Fig. 13 compares the MRAOs when using the three coupling strategies. It is observed that higher wave encounter frequencies, the quasistatic and weak couplings fail to recover the resonance effect. And for encounter frequencies around three times smaller than resonance, all coupling strategies provide similar results.

6.4. Hydroelastic analysis in irregular waves

Next, a structural analysis is carried out in irregular waves to compare the coupling strategies. Table 7 provides the wave spectral data. The spectrum has been discretized using 1000 regular waves, with a minimum wave period of 1 s and a maximum wave period of 6.25 s. This corresponds to a minimum and maximum wave encounter frequencies of 0.24 Hz and 4.28 Hz respectively (see Fig. 14). Looking at *Fig. 13* right, wave loads are in the resonance range of the 1st mode, and therefore a strong coupling strategy is required to capture resonance effects. The minimum wave encounter period is 0.233 s. Hence, a time step of 0.025 s is selected to properly capture the higher frequency responses.

For the structural solver a Rayleigh damping model has been used with:

- $\alpha_M = 0$
- $\alpha_K = 2 \cdot 0.01/(2\pi f_1) = 6.89 \cdot 10^{-4}$,

where $f_1 = 4.55\ Hz$ is the modal frequency of the first mode. Hence, the relative modal damping for every mode is:

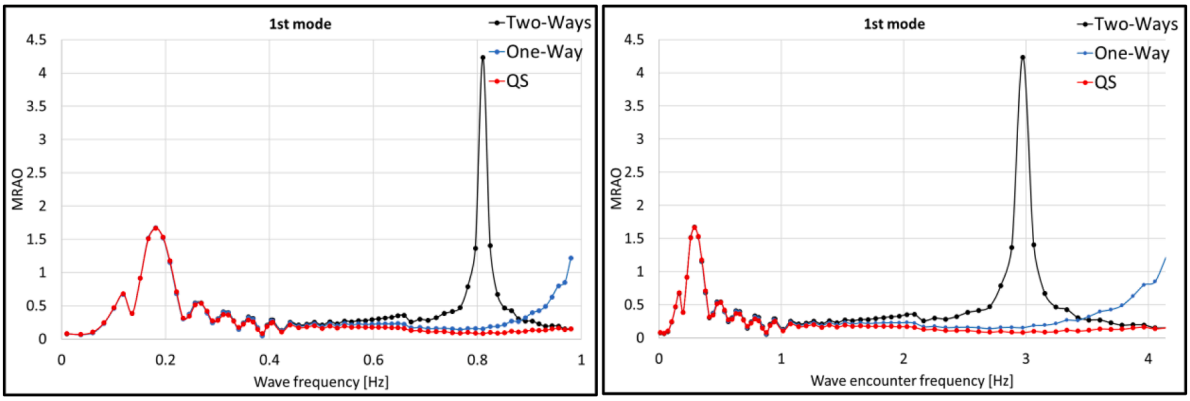

Fig. 13. Modal RAOs at 10 knots in head waves: Left: MRAOs vs wave frequency; Right: MRAO vs wave encounter frequency.

Table 7
Irregular waves scenarios.

Velocity	Wave direction	Spectrum	H_s	T_m
10 Kts	180°	JONSWAP	1.0 m	2.5 s

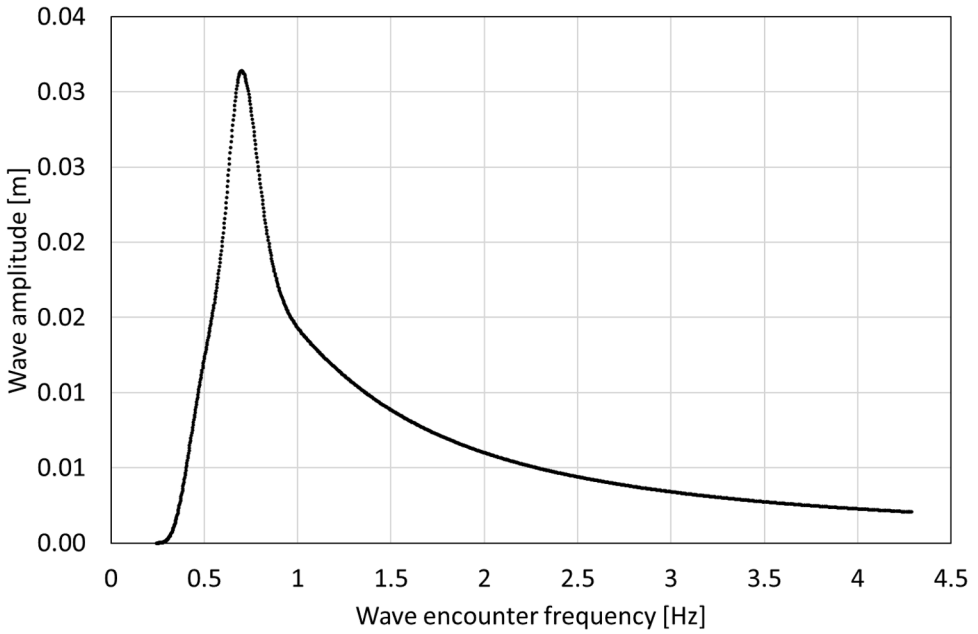

Fig. 14. JONSWAP spectrum discretization versus wave encounter frequency.

- $\eta_i = \alpha_K \cdot \frac{(2\pi f_i)}{2} = 0.01 \cdot \frac{f_i}{f_1}$.

Fig. 15 compares the dynamic elastic energy computed using Eq. (25) for different coupling strategies. It is observed that the quasistatic and the weak coupling fail to recover the strong coupling solution because the wave encounter frequencies are in the resonance frequency range.

Fig. 16 compares the dynamic elastic energy using the 2 ways coupling strategy with FOM and ROM with different sizes of the modal basis. It is observed how as the size of the modal basis increases (from 30 modes to 5000 modes) the solution converges with the FOM solution.

Fig. 17 compares the dynamic elastic energy using the strong ROM coupling against the hybrid strategy reported in Section 3, where the strong ROM coupling is combined with weak ROM coupling for the residual system. It is observed that in all cases, similar values of dynamic energy are obtained.

Table 8 reports the computational times required to solve the rigid body dynamics and the structural dynamics using the different approaches reported in this research. The data is presented in terms of seconds of computation per second of physical time (e.g., 1.0 indicates real-time performance). The computations have been performed using a single workstation with an AMD Ryzen Threadripper PRO 5995WX 2.70 Ghz processor unit. And OpenMP has been used for parallel computing using 8 threads.

Using the dynamic strong FOM solution as a reference, significant computational times reduction can be obtained using the strong ROM approach with 5000 modes and the hybrid ROM-FOM couplings, while yet obtaining similar high-fidelity solutions. Moreover, the use of ROM approach can provide insightful information into which modes are predominantly excited.

As mentioned earlier, previous studies have reported that most of the computational time required for fully coupled analyses based on potential flow hydrodynamics is spent on solving structural dynamics [35,48]. Therefore, the time reductions achieved by the proposed hybrid approach, respect to the strong FOM, reach up to 8 × for hybrid-FOM, and up to 125 × for Hybrid-ROM without significant loss of accuracy. These speed-ups are highly relevant.

It is worth noting that the structural model adopted in this case study is simplified, which leads to the use of a relatively coarse mesh. For more detailed structural models, the computational time required for hydro-elastic analyses is expected to increase significantly, making the achieved time reductions even more relevant. Moreover, in such refined models, the structural solver's computation time is likely to dominate over that of the wave diffraction–radiation problem. To illustrate this, a refined structural mesh was used, increasing the number of structural degrees of freedom by approximately a factor of four compared to the previous case. The particulars of the FEM mesh used in this configuration are provided in Table 9. It is also noted that, in both cases, the computational time of the wave diffraction–radiation solver remains unchanged at 40.32 s s^{-1}.

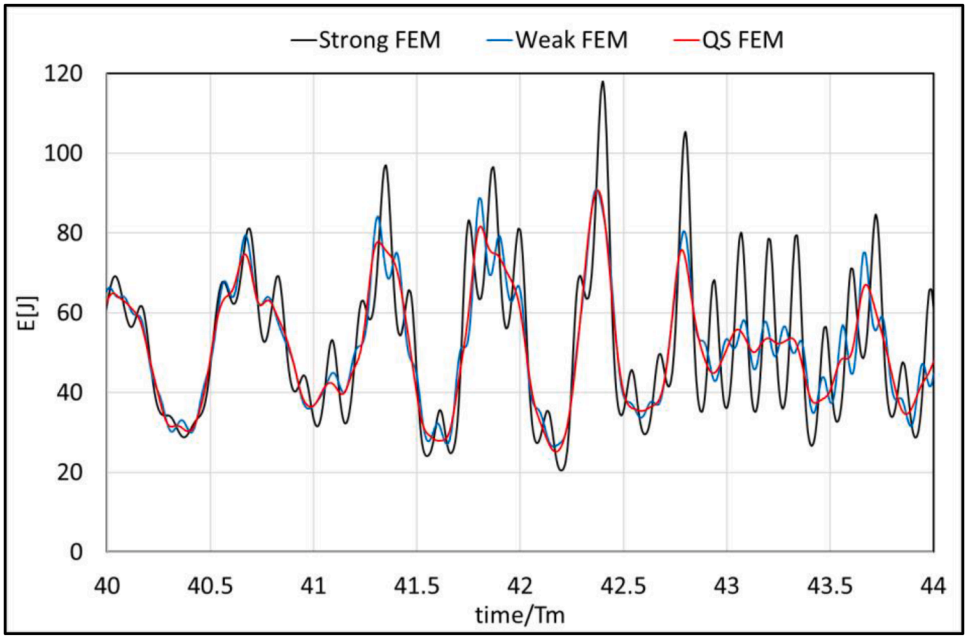

Fig. 15. Comparison of dynamic energy computed using FOM and different coupling strategies.

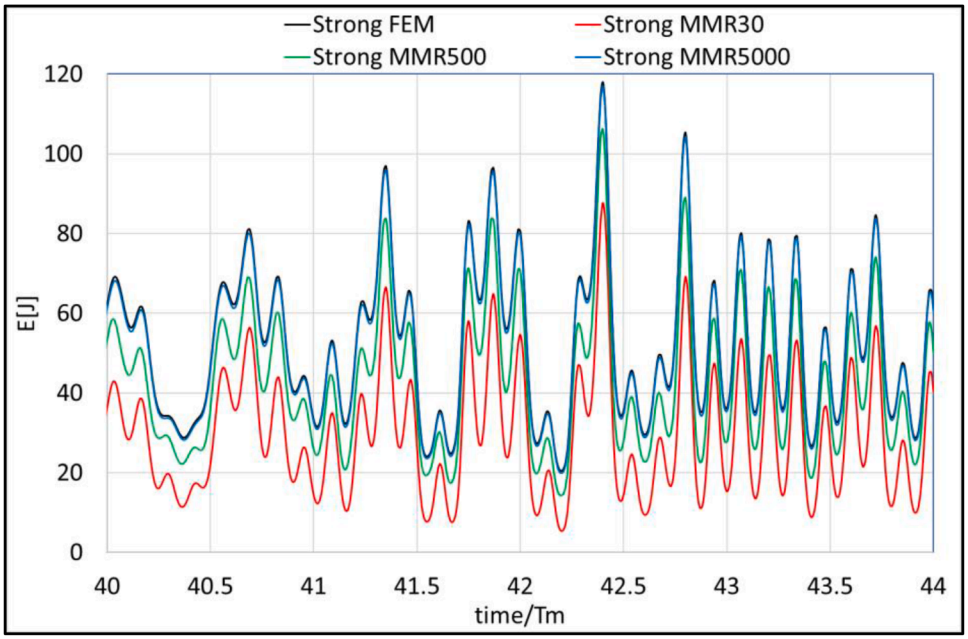

Fig. 16. Comparison of dynamic energy computed using 2-ways coupling, FEM and MMR.

Table 10 provides a summary of the computational times for the refined structural mesh. In this case, the time reduction remains around 8 × for the hybrid-FOM and increases up to 300 × for the hybrid-ROM compared to the full FOM.

In larger ships, where elastic responses become more significant, the use of strong coupling will be necessary for a wider range of load case scenarios. In any case, the application of ROM and hybrid strategies can help reduce considerably the computational effort required while still providing the necessary accuracy.

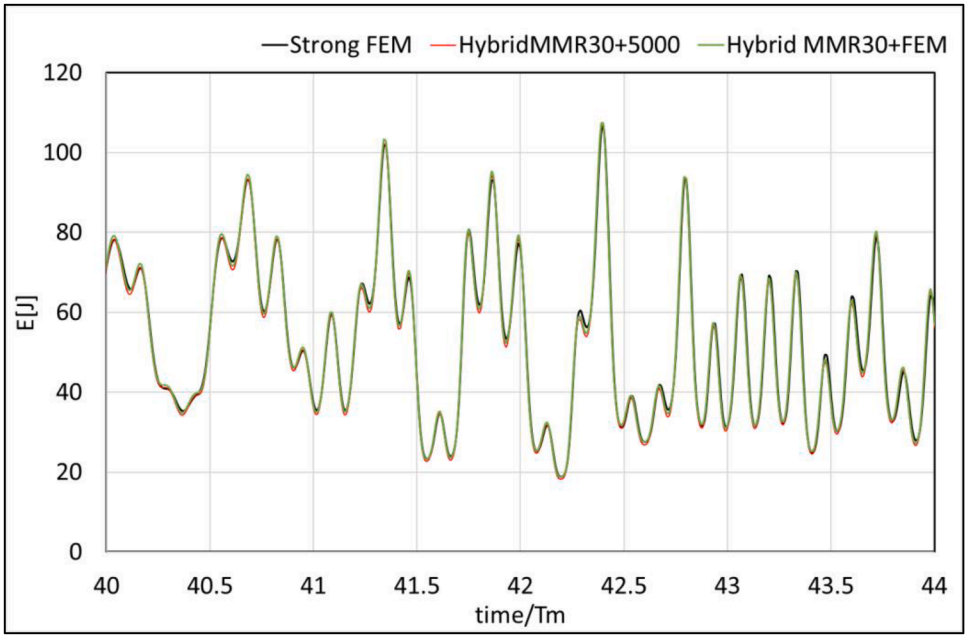

Fig. 17. Comparison of dynamic energy: strong FEM versus hybrid couplings.

Table 8
Computational times in second per second of simulation.

Structural solver	Type of Coupling	Model order	Solver	Computational time
	Quasistatic	ROM	MMR5000	0.23 s s^{-1}
	Quasistatic	FOM	FEM	8.27 s s^{-1}
	Weak	ROM	MMR5000	0.23 s s^{-1}
	Weak	FOM	FEM	8.23 s s^{-1}
	Strong	ROM	MMR5000	10.74 s s^{-1}
	Strong	FOM	FEM	71.74 s s^{-1}
	Hybrid	ROM	MMR30–5000	0.57 s s^{-1}
	Hybrid	FOM	MMR30+FEM	8.41 s s^{-1}
Rigid body solver				0.03 s s^{-1}

Table 9
Structural Mesh 2 particulars.

Number of FE elements	170,568
Number of nodes	157,245
Number of DOF	943,470

Table 10
Computational times in second per second of simulation.

Structural solver	Type of Coupling	Model order	Solver	Computational time
	Quasistatic	ROM	MMR5000	0.93 s s^{-1}
	Quasistatic	FOM	FEM	47.91 s s^{-1}
	Weak	ROM	MMR5000	0.94 s s^{-1}
	Weak	FOM	FEM	47.79 s s^{-1}
	Strong	ROM	MMR5000	26.96 s s^{-1}
	Strong	FOM	FEM	398.87 s s^{-1}
	Hybrid	ROM	MMR30–5000	1.34 s s^{-1}
	Hybrid	FOM	MMR30+FEM	48.63 s s^{-1}
Rigid body solver				0.03 s s^{-1}

7. Conclusions

This work has presented an innovative numerical framework for fully (two-way) coupled hydro-elastic analysis of ships navigating with forward speed. However, the computational resources required to solve a fully coupled problem can be prohibitively high for practical applications. To overcome this bottleneck, the developed structural solver has been reduced using the MMR technique. The use of a single time-domain computational framework based on FEM allows for more efficient strong hydro-elastic coupling, avoiding file-based communication between different solvers.

The consistency of the ROM based on the MMR has been verified comparing against FOM solution for the hydrostatic equilibrium condition, finding a very good agreement. For the present application, a modal basis of 5000 eigenmodes has been considered to accurately recover the elastic structural energy. The ROM implies a large reduction in the number of structural DOFs from 235,116 of the FOM model to 5000 DOFs (modes). This results in a reduction of approximately 98 % in the number of DOFs. And there is still room for further reduction of the modal basis if only most energetic modes are considered. And this reduction will be proportional to the number of modes used.

However, when ROM is applied with a limited number of modes, the accuracy can degrade, especially in capturing structural details. To overcome this drawback, this work proposes a combined methodology in which a residual FEM solution is computed alongside the reduced model, still achieving a reduction in the overall computational effort required.

The ROM approach allows for offline computation of structural displacements and stresses. These are computed from the modal amplitudes and the modal basis. Then, the instantaneous structural energy allows for the detection of the critical time instants. At these, the hotspots of maximum stress can be identified. This avoids the need to compute the stresses over the full structure along the whole simulations. Instead, the structural response can be obtained over the whole structure at critical time instants, and for every time step at specific hotspots. This implies a more precise analysis and a large reduction of output data.

On the one hand, when considering wet from dry conditions, a significant change in the modal frequency is observed for the lower modes. Strong, weak, and quasi-static couplings have been compared. While strong coupling makes it possible to recover the hydroelastic response under near-resonance conditions, the results show that one-way and quasi-static approaches can lead to significant errors, especially when the wave encounter frequency approaches modal resonance.

Modal response amplitude operators (MRAOs) have been obtained under head waves loading. As the first bending mode is the most energetic mode under this condition, it has been used for an energy analysis to compare the quasistatic, weak and strong couplings. Large resonance effects are detected, inducing large differences for wave frequency near modal resonance. Moreover, differences between the weak and strong coupling are also significant due to the change in the modal frequency from dry to wet conditions.

The case study has demonstrated that the use of MMR and hybrid solutions can deliver accurate results (comparable to those obtained with the full FEM solution) while significantly reducing computational time. Furthermore, for linear problems, computing the MRAOs across a range of wave directions, frequencies, and ship forward velocities can generate a dataset of precomputed results, allowing any scenario to be quickly evaluated using that information.

In practical terms, the ability of the developed methodology to accurately predict strong-coupling hydro-elastic responses in near-real-time under operational conditions provides a foundation for advanced applications. On one side, the reduced computational cost facilitates the integration of the methodology into iterative design loops, providing an efficient and accurate approach for strength and fatigue assessment of naval structures based on full-length detailed models. On the other hand, it enables integration with onboard monitoring systems, making it a promising tool for next-generation digital twin solutions. This capability is essential for monitoring fatigue, detecting critical loading events, and supporting operational and maintenance decision-making, ultimately enhancing the safety and reliability of ship structures throughout their service life.

Funding

This research was funded by the Spanish “Ministerio de Ciencia e Innovacion”, via “Agencia Estatal de Investigación (AEI)”, under the grant agreement MLAMAR (ref. PID2021–126561OB-C31).

CRediT authorship contribution statement

Julio García-Espinosa: Writing – original draft, Supervision, Methodology, Conceptualization. **Antonio José Lorente-López:** Writing – review & editing, Validation, Methodology. **Borja Serván-Camas:** Writing – original draft, Supervision, Methodology, Funding acquisition, Conceptualization. **José Enrique Gutierrez-Romero:** Writing – review & editing, Validation, Methodology.

Declaration of competing interest

The authors declare that they have no known competing financial interests or personal relationships that could have appeared to influence the work reported in this paper.

Acknowledgements

The structural FEM model used in this study has been kindly provided by Navantia and Maestro Marine, and the authors gratefully acknowledge their support.

Data availability

Data will be made available on request.

References

[1] Inglis CE. Natural frequencies and modes of vibration in beams of non-uniform mass and section. Trans R Instn Nav Archit 1929;72:66–145.
[2] Bishop RED, Price WG. Hydroelasticity of ships. Cambridge: Cambridge University Press; 1979.
[3] Bishop RED, Price WG, Wu Y. A general linear hydroelasticity theory of floating structures moving in a seaway. Philos Trans R Soc A: Math Phys Eng Sci 1986; 316(1538):375–426. https://doi.org/10.1098/rsta.1986.0016.
[4] Malenica S. Hydro structure interactions in seakeeping. Dubrovnik, Croatia: International workshop on coupled methods in numerical dynamics IUC; 2007. September 19th-21st.
[5] Maron A, Kapsenberg G. Design of a ship model for hydro-elastic experiments in waves. 1130~1147. Int J Nav Arch Ocean Eng 2014;6. https://doi.org/10.2478/IJNAOE-2013-0235.
[6] Watanabe I, Ueno M, Sawada H. Effects of bow flare shape to the wave loads of a containership. J Soc Nav Arch Jpn 1989;166:66–259.
[7] Hay B, Bourne J, Engle A, Rubel R. Characteristics of hydrodynamic loads data for a naval combatant. 1994. Trondheim Hydroelasticity Mar Technol 1994; 22–28:88–169. May 1994.
[8] Iijima K, Hermundstad OA, Zhub S, Moan T. Symmetric and antisymmetric vibrations of a hydroelastically scaled model. Hydroelasticity Mar Technol 2009:173 1382 2009. 8-10 September 2009.
[9] Mahérault S, Derbanne Q, Bigot F. Fatigue damage calculation of ULCS based on hydroelastic model for springing. Sh Offshore Struct 2013;8(Nos. 3–4): 289–302. https://doi.org/10.1080/17445302.2012.750087.
[10] Kim J-H, Kim Y, Korobkin A. Comparison of fully coupled hydroelastic computation and segmented model test results for slamming and whipping loads. Int J Nav Arch Ocean Eng 2014;6:81–1064.
[11] Kim n Y, Kim J-H. Benchmark study on motions and loads of a 6750-TEU containership. Ocean Eng 2016:73–262. 2016.
[12] Chen Z, Gui H, Dong P. Nonlinear time-domain hydroelastic analysis for a container ship in regular and irregular head waves by the Rankine panel method. Sh Offshore Struct 2018. https://doi.org/10.1080/17445302.2018.1535243.
[13] Jiao J, Chen C, Ren H. A comprehensive study on ship motion and load responses in short-crested irregular waves. Int J Nav Archit Ocean Eng 2018 2019;11: 364–79.
[14] Jiao J, Jiang Y, Zhang H, Li C, Chen C. Predictions of ship extreme hydroelastic load responses in harsh irregular waves and hull girder ultimate strength assessment. Appl Sci 2019;9:240. https://doi.org/10.3390/app9020240. 2019.
[15] Mursid O, Oterkus E, Oterkus S. Coupled ship simulation in hydrodynamics and structural dynamics induced by wave loads: a systematic literature review. J Mar Sci Eng 2025;13(3):447. https://doi.org/10.3390/jmse13030447.
[16] Ki-Ho S, Jo J, E HS, Jeong S, Bum PJ, Frank L, Zhenhong W, Nigel W. Two- and three-dimensional springing analysis of a 16,000 TEU container ship in regular waves. Sh Offshore Struct 2015;10(5):498–509. Conference on Hydroelasticity in Marine Technology; 2015. p. 457–76.
[17] Kim Y., Kim J.H., Kim Y. Development of a highfidelity procedure for the numerical analysis of ship structural hydroelasticity. Split, Croatia: 7th international.
[18] Datta R, Guedes Soares C. Analysis of the hydroelastic effect on a container vessel using coupled BEM–FEM method in the time domain. Sh Offshore Struct 2019. https://doi.org/10.1080/17445302.2019.1625848.
[19] Jagite G, Xiang-Dong X, Xiao-Bo C, Sime M. Hydroelastic analysis of global and local ship response using 1D–3D hybrid structural model. Sh Offshore Struct 2018. https://doi.org/10.1080/17445302.2018.1425521.
[20] Oberhagemann J, Shigunov V, Radon M, Mumm H, Won SI. Hydrodynamic load analysis and ultimate strength check of an 18000 TEU containership. In: Split, croatia: 7th international conference on hydroelasticity in marine technology; 2015. p. 591–606.
[21] Craig M, Piro D, Schambach L, Mesa J, Kring D, Maki K. A comparison of fully coupled hydroelastic simulation methods to predict slam induced whipping. In: Split, Croatia: 7th International Conference on Hydroelasticity in Marine Technology; 2015. p. 90–575.
[22] Lakshmynarayanana PA, Temarel P, Chen Z. Coupled fluid-structure interaction to model three dimensional dynamic behaviour of ship in waves. In: 7th international conference on hydroelasticity in marine technology; 2015. p. 36–623.
[23] Im HI, Vladimir N, Malenica S, Ryu HR, Cho DS. Fatigue analysis of HHI SkyBenchTM 19000 TEU ultra large container ship with springing effect included. In: Split, Croatia: 7th international conference on hydroelasticity in marine technology; 2015. p. 74–561.
[24] Patalano S, Mango Furnari A, Vitolo F, et al. A critical exposition of model order reduction techniques: application to a slewing flexible beam. Arch Comput Methods Eng 2021;28:31–52. https://doi.org/10.1007/s11831-019-09369-1.
[25] Lee H, Moon W, Lee M, et al. Time-domain response-based structural analysis on a floating offshore wind turbine. J Mar Sci Appl 2023;22:75–83. https://doi.org/10.1007/s11804-023-00322-0.
[26] Lee H, Kim J, Kim J, Shen Z, Kyoung J, Baquet A, Lee H, Kim JW. An efficient time domain structural assessment of a floating wind turbine structure. In: Proceedings of the 42nd international conference on ocean, offshore and arctic engineering (OMAE 2023). ASME; 2023. https://doi.org/10.1115/OMAE2023-108155.
[27] DNV. In: Sesam floating wind time domain — release note; 2024. June[Online]Available, https://mysoftware.dnv.com/download/public/sesam/sesam-workflows/whatsnew/SesamFloatingWindTimeDomainReleaseNote_June2024.pdf.
[28] Cummins WE. The impulse response function and ship motions. Schiffstecknik 1962.
[29] Kim SJ, Jin C, Lee I, Kim GJ, Kim MH, Kwak HG. Efficient time-domain approach for hydroelastic-structural analysis including hydrodynamic pressure distribution on a moored SFT. Mar Struct 2023;90:103–402. https://doi.org/10.1016/j.marstruc.2023.103402.
[30] Amouzadrad P, Mohapatra SC, Guedes Soares C. Review of recent developments on the hydroelastic response and gap resonance of multi-body floating structures. Ocean Eng 2024;313:119–398. https://doi.org/10.1016/j.oceaneng.2024.119398.
[31] Hess P. Fluid structure interaction: a community view. MSDL report number: 2016-003. 2016.
[32] Garcia-Espinosa J, Di Capua D, Servan-Camas B, Ubach P-A, Eu O. A FEM fluid–structure interaction algorithm for analysis of the seal dynamics of a Surface-Effect Ship. Comput Methods Appl Mech Eng 2015;295:290–304.
[33] Lakshmynarayanana PAK, Hirdaris S. Comparison of nonlinear one- and two-way FFSI methods for the prediction of the symmetric response of a containership in waves. Ocean Eng 2020;203:107–79. https://doi.org/10.1016/j.oceaneng.2020.107179.
[34] Tavakoli S, Singh M, Hosseinzadeh S, Hu Z, Shao Y, Wang S, Huang L, Grammatikopoulos A, Li YP, Khojasteh D, Liu J, Dolatshah A, Cheng H, Hirdaris S. Ocean Engineering, 342, a review of flexible fluid-structure interactions in the ocean: progress, challenges, and future directions. Ocean Eng 2025. https://doi.org/10.1016/j.oceaneng.2025.122545.
[35] Servan-Camas B, Di-Capua D, Garcia-Espinosa J, Sa-Lopez D. Fully 3D ship hydroelasticity: monolithic versus partitioned strategies for tight coupling. J Mar Struct Vol 2021;80:103098. https://doi.org/10.1016/j.marstruc.2021.103098.
[36] Colomés O, Verdugo F, Akkerman I. A monolithic finite element formulation for the hydroelastic analysis of very large floating structures. Int J Numer Methods Eng 2022;124(3):51–714. https://doi.org/10.1002/nme.7140.
[37] Sim K, Kim B, Han J, Lee K. Structural response evaluation of krylov subspace-based reduced-order model for real-time structural health monitoring and prediction of container ships. J Ocean Eng Technol 2025. https://doi.org/10.26748/ksoe.2025.002.
[38] Servan-Camas B, García-Espinosa J. Accelerated 3D multi-body seakeeping simulations using unstructured finite elements. J Comput Phys 2013;252:382–403. https://doi.org/10.1016/j.jcp.2013.06.023 [Google Scholar].

[39] Servan-Camas B. A time-domain finite element method for seakeeping and wave resistance problems- Doctoral Thesis. School of Naval Architects and Marine Engineers. Technical University of Madrid; 2016 [Google Scholar] [View PDF].
[40] Garcia-Espinosa J, Di Capua D, Servan-Camasa B, Ubach P-A, Oñate E. A FEM fluid–structure interaction algorithm for analysis of the seal dynamics of a surface-effect ship. J Comput Methods Appl Mech Engrg 2015;295:290–304. https://doi.org/10.1016/j.cma.2015.07.010 [Google Scholar].
[41] Gutierrez-Romero JE, García-Espinosa J, Servan-Camas B, Zamora-Parra B. Non-linear dynamic analysis of the response of moored floating structures. J Mar Struct 2016;49:116–37. https://doi.org/10.1016/j.marstruc.2016.05.002 [Google Scholar].
[42] Serván-Camas B, Cercós-Pita JL, Colom-Cobb J, García-Espinosa J, Souto-Iglesias A. Time domain simulation of coupled sloshing–seakeeping problems by SPH–FEM coupling. J Ocean Eng 2016;123:96–383. https://doi.org/10.1016/j.oceaneng.2016.07.003 [Google Scholar].
[43] Servan-Camas B, Gutierrez-Romero JE, García-Espinosa J. A Time-domain second-order FEM model for the wave diffraction-radiation problem. Validation with a semisubmersible platform. Mar Struct 2018;58:278–300. https://doi.org/10.1016/j.marstruc.2017.12.001 [Google Scholar].
[44] Garcia-Espinosa, J.; Servan-Camas, B. 2018 A non-linear finite element method on unstructured meshes for added resistance in waves. J Sh Offshore Struct DOI: 10.1080/17445302.2018.1483624 [Google Scholar].
[45] Garcia-Espinosa J, Servan-Camas B, Calpe-Linares M. High fidelity hydroelastic analysis using modal matrix reduction. J Mar Sci Eng 2023;11:1168. https://doi.org/10.3390/jmse11061168 [Google Scholar].
[46] https://www.compassis.com/compass/es/Productos/SeaFEM.
[47] https://www.compassis.com/compass/es/Productos/RamSeries.
[48] Servan-Camas B, Berdugo-Parada I, Garcia-Espinosa J, Pastor-Sanchez A. Modal matrix reduction for fully coupled integrated load analysis of floating structures. Mar Struct 2025;103:103845. https://doi.org/10.1016/j.marstruc.2025.103845.modal.
[49] Bathe, K.J. Finite element procedures. K.J. Bathe, Watertown, MA. (2016).
[50] Irons BM, Tuck RC. A version of the Aitken accelerator for computer iteration. Int J Numer Methods Eng 1969;1:7–275.